Whole genome CRISPR screens identify a LRRK2-regulated pathway for extracellular tau uptake by human neurons

Lewis D. Evans[1,2,3], Alessio Strano[1,4], Eleanor Tuck[1,2,3], Ashley Campbell[1,2], James Smith[1,9], Christy Hung[1], Tiana S. Behr[5], Bernardino Ghetti[6], Benjamin Ryskeldi-Falcon[5], Emre Karakoc[2,7], Francesco Iorio[2,7], Alastair Reith[8], Andrew R. Bassett[2,3], and Frederick J. Livesey[1,9*]

[1]UCL Great Ormond Street Institute of Child Health, Department of Developmental Biology and Cancer, Zayed Centre for Research into Rare Disease in Children, London WC1N 1DZ, UK

[2] Open Targets, Wellcome Genome Campus, Cambridge CB10 1SA, UK.

[3] Wellcome Sanger Institute, Wellcome Genome Campus, Cambridge CB10 1SA, UK.

[4] Department of Biosystems Science and Engineering, ETH Zurich, Basel, Switzerland

[5] MRC Laboratory of Molecular Biology, Cambridge, CB2 0QH, UK.

[6] Department of Pathology and Laboratory Medicine, Indiana University School of Medicine, Indianapolis, IN, USA

[7] Human Technopole, 20157, Milano Italy.

[8] Novel Human Genetics Research Unit, GlaxoSmithKline Pharmaceuticals R&D, Stevenage, UK

[9] Talisman Therapeutics, Babraham Research Campus, Cambridge CB22 3AT, UK

[*]Author for correspondence: rick@talisman-therapeutics.com

Abstract

Extracellular release and cellular uptake of pathogenic forms of the microtubule-associated protein tau contribute to the pathogenesis of several neurodegenerative diseases, including Alzheimer's disease. Defining the cellular mechanisms and pathways for tau entry to human neurons is essential to understanding tauopathy pathogenesis and the rational design of disease-modifying therapeutics. Whole genome CRISPR loss-of-function screens in human iPSC-derived excitatory neurons, the major neuronal cell type affected in these diseases, enabled the delineation of the different cellular pathways for uptake of extracellular monomeric and fibrillar tau. Monomeric and fibrillar tau are both taken up by human neurons by receptor-mediated endocytosis, but involve different routes of entry at the neuronal surface: the low-density lipoprotein LRP1 is the primary receptor for monomeric tau, but contributes less to fibrillar tau entry. Similarly, endocytosis of monomeric tau is dependent on the familial Parkinson's disease gene LRRK2, but not required for endocytosis of fibrillar tau. These findings implicate LRP1 and LRRK2 in the pathogenesis of tauopathies and Parkinson's disease and identify LRRK2 as a potential therapeutic target for altering progression of these diseases.

Main

Neurodegenerative diseases that involve the microtubule-associated protein tau (tau, *MAPT*), such as Alzheimer's disease, corticobasal degeneration and progressive supranuclear palsy, are referred to collectively as tauopathies[1]. Characterised by the formation of intracellular aggregates of tau protein, these diseases also display stereotyped spatiotemporal progression of pathology through the central nervous system, including the cerebral cortex[2,3]. The spatial progression of tau aggregation mirrors the connectivity of the central nervous system[4], and the involvement of different brain regions at different stages of disease is reflected in the development of clinical symptoms. A current working model for tauopathy progression is that pathogenic forms of tau protein are released from diseased neurons containing tau protein aggregates. These are either taken up by synaptically-connected neurons or processed and released by microglia before subsequent uptake by neurons[5]. In both cases, pathogenic forms of tau are hypothesised to be transferred to surrounding neurons, seeding further tau aggregation and neuronal dysfunction[3].

There is considerable interest in identifying the forms of tau and associated molecules that mediate disease progression and the biological mechanisms involved in potential intercellular tau transfer, including cell surface receptors. In addition to understanding disease pathogenesis, such insights are essential to the rational design of therapies to slow disease progression[4]. It is currently not known which forms of tau mediate the proposed pathogenic spreading of tauopathy between neurons[6], although oligomers and fibrillar aggregates of either full length tau or fragments that include the microtubule-binding region are considered strong candidates[7]. While the identity of the pathogenic tau species responsible for disease propagation remains unknown, progress has been made in understanding the mechanisms of cellular uptake of tau[2]. Cell surface heparan sulfate proteoglycans have been found to be necessary for uptake of tau fibrillar aggregates[8], and we and others have found that human neurons efficiently take up both monomeric and fibrillar tau by overlapping but distinct mechanisms, consistent with dynamin-dependent receptor-mediated endocytosis[9,10]. More recently, the low-density lipoprotein receptor LRP1 has been identified as a major neuronal receptor for monomeric and oligomeric tau uptake via receptor-mediated endocytosis[11].

To define the cell biology of neuronal uptake of extracellular tau, we used whole-genome CRISPR loss-of-function screens in human iPSC-derived cortical excitatory neurons to identify genes and pathways required for neuronal uptake of tau protein. Given the accumulating evidence that different forms of monomeric, oligomeric and fibrillar tau may contribute to disease pathogenesis[12–14], we carried out whole genome CRISPR knockout

screens[15] for genes required for neuronal uptake of either full-length monomer or fibrillar aggregates of tau[9]. Previous work has indicated that tau monomers and oligomers both are endocytosed via the LRP1 receptor[11], thus for screening purposes we used monomeric full-length tau to represent both monomeric and oligomeric tau. We also carried out screens for uptake of fibrillar, aggregated tau, which we and others have previously shown enters human neurons via a pathway distinct to that of monomeric tau[9,16]. These screens were performed using human iPSC-derived cerebral cortex excitatory neurons[17], the primary cell type affected by tau aggregation into neurofibrillary tangles *in vivo*[1]. Intraneuronal levels of internalised, fluorescently-labelled tau were assessed acutely, limiting the relative importance of degradation of tau protein. As reported in detail below, genome-wide loss of function genetic screens identified key elements of the different pathways for neuronal entry used by monomeric and fibrillar tau, providing tractable therapeutic targets for disease intervention.

Results

FACS-based CRISPR knockout screens in human neurons to identify genes and pathways required for uptake of extracellular tau

We have previously found that fibrillar and monomeric tau are taken up by human neurons by overlapping, but distinct pathways[9]. CRISPR knockout screens of human neuronal uptake of extracellular tau were designed using the approach outlined (Fig. 1a). Cerebral cortex progenitor cells were generated from human iPSCs constitutively expressing Cas9 from the AAVS1 locus, using our previously described methods[18], and differentiated to cortical excitatory neurons (Fig. 1b; Extended Data Fig. 1). Using a lentiviral reporter of Cas9 activity, we found that gene editing of the KOLF2-C1 Cas9 neurons increased over time to >35% efficiency (Fig. 1c, d).

To identify and compare the cellular pathways by which monomeric and fibrillar P301S tau enter neurons, FACS-based assays were optimised to measure uptake of both forms of tau by human iPSC-derived cortical excitatory neurons. To focus the screens on genes required specifically for tau uptake, and not general mechanisms of receptor-mediated endocytosis, assays were designed to measure uptake of transferrin and tau by the same neurons (Fig. 1). Transferrin endocytosis was confirmed not to affect tau uptake at a range of concentrations (Fig. 1e, f), and thus not interfere with the screen readout.

For the screens, a lentivirus library composed of 100,090 gRNAs, targeting 18,025 genes[15], was introduced by transducing cortical progenitor cells with lentivirus at an MOI of 0.3, and progenitor cells subsequently differentiated to cortical excitatory neurons for 30 days. To identify lentivirus-transduced, guide RNA-expressing neurons that failed to take up tau but remained competent to endocytose transferrin, neurons were exposed to extracellular tau (labelled with Dylight-488) and transferrin (conjugated with Alexa-633) for either 4 or 5 hours, before being dissociated to single cells and fixed. Lentivirus-transduced, gRNA-expressing neurons were gated, the populations of neurons with high transferrin protein uptake that also had either high or low tau uptake were collected (Fig. 1g, Extended Data Fig. 1, Supplementary Table 1) and gRNA abundance in each population measured using high throughput sequencing.

CRISPR screens identify genes and pathways required for human neuronal uptake of monomeric and fibrillar tau

Replicate screens for monomeric and fibrillar tau uptake were analysed using the MAGeCK algorithm[19] to identify genes whose loss of function results in reduced neuronal tau uptake (Fig. 2; Extended Data Fig. 2). Applying a significance cutoff of $p<0.01$ identified 214 genes

required for monomeric tau uptake and 228 genes required for fibrillar tau uptake. The low density lipoprotein receptor LRP1, which has been shown to act as a tau receptor[11] was the second-highest ranked gene identified in the monomeric tau uptake screens, supporting the validity of the loss of function screen design.

For monomeric tau uptake, the most highly ranked gene was *LRRK2*, a large multifunctional protein that regulates diverse intracellular vesicle trafficking processes, mutations in which are a cause of autosomal dominant Parkinson's disease (PD)[20]. In addition to *LRRK2*, there was a notable number of genes required for monomeric tau uptake encoding regulators of endocytosis, including AP2 subunits (*AP2M1*, *AP2S1*), dynamin-2 (*DNM2*), clathrin heavy chain (*CLTC*), *RAB7A*, *HGS* and PI3 kinase subunits C3 and R4. Several genes involved in endosomal sorting, such as *SNX16*, and specifically recycling of the LRP1 receptor were also required for monomeric tau uptake, including *SNX17*[21] and the LDL receptor chaperone *MESD*/*MESDC2*[22]. In addition, genes involved in lysosome and autophagosome biogenesis and acidification were prominent, including the vATPase subunit *ATP6V1D*, the vATPase assembly protein *VMA21*[23], and the autophagy regulating proteins UVRAG and ATG4A[24].

In addition to individual genes, gene ontology and pathway analyses of the set of genes required for monomeric tau uptake provides a useful overview of the cellular mechanisms involved. Gene ontology and functional analysis of the set of genes above the empirical significance threshold of $p<0.01$ found significant enrichment in several categories related to receptor-mediated endocytosis, including lipoprotein particle receptor binding, the endosome, clathrin-coated pit and the autolysosome (Fig. 2b).

Using the same significance cutoff of $p<0.01$ as for analysis of the monomeric tau screen identified 228 genes required for fibrillar tau uptake (Fig. 2c). *LRP1* did not reach that threshold ($p=0.024$), suggesting that it is not a major receptor for fibrillar tau. As for monomeric tau, genes required for neuronal uptake of fibrillar tau include regulators of endocytosis, but in this case *EEA1* and *HGS,* and the PI3 kinase subunits C3 and R4. Similarly, genes encoding vATPase subunits were required for fibrillar tau uptake (*ATP6V0E2, ATP6V0D1, ATP6V0A1*), as were autophagy genes such as *GABARAPL1* and *UVRAG* (Fig. 2c). Several genes encoding proteins involved in intracellular vesicular trafficking were required for fibrillar tau uptake, including the AP-1 and AP-3 complexes (*AP1G1, AP3S1*), and the COG complex that regulates retrograde trafficking within the Golgi[25] (four of the eight COG subunits: 1, 4, 7 & 8). Gene ontology and functional analysis identified categories enriched in the set of genes required for fibrillar tau uptake, including

endosomal transport, the COG complex, Golgi vesicle transport, vacuolar acidification, the autophagosome and the CCC-WASH complex (Fig. 2d).

A subset of genes identified as required for uptake of monomeric tau was subsequently validated by targeted, lentivirus-mediated CRISPR knockout in iPSC-derived neural progenitor cells, followed by differentiation to excitatory neurons (Fig 2e, f). The effect of each CRISPR knockout on uptake of extracellular fluorescently-labelled tau and transferrin was measured by FACS, using the primary metric of the fraction of neurons with reduced tau uptake (tau-low/transferrin+ neurons) relative to the population of neurons that took up both tau and transferrin (Fig 2e, example shown of AP2M1). Validated genes using this assay included the LRP1 receptor, both AP2 adaptor subunits AP2M1 and AP2S1, dynamin-2 (DNM2) and two PI3-kinase components (PIK3C3 and PIK3R4).

LRP1 has recently been identified as a major tau receptor for both monomeric and oligomeric tau[11], and was one of the two most significant genes identified as required for monomeric tau entry in our screens. We confirmed that LRP1 is required for monomeric tau uptake by CRISPR knockout of LRP1 in iPSC-derived neural progenitor cells, using the FACS-assay for uptake of extracellular tau and transferrin (Fig 2f). However, LRP1 did not meet the threshold for inclusion as a gene required for fibrillar tau entry (ranked 522 of 18,019 genes; p=0.024), consistent with previous reports[11].

To test the dependency of monomeric and fibrillar tau entry on interaction with LRP1, we used two different approaches to inhibiting tau-LRP1 interactions, combined with live-imaging of neuronal uptake of pHrodo-labelled tau. Blockade of all LDL receptors by addition of the pan-LDL receptor chaperone RAP[26] reduced uptake of monomeric tau by approximately 63%, with a minor effect on fibrillar tau (Fig. 2g-i; Extended Data Fig. 3). As an alternative approach to inhibiting tau interactions with cell surface LRP1, we added soluble recombinant domain IV of LRP1, the region defined as binding tau[11], together with pHrodo-tau, and subsequently imaged tau uptake (Fig. 3a-c; Extended Data Fig. 3). As with RAP, the addition of the LRP1 fragment reduced uptake of monomeric tau by approximately 68% (Fig. 3a-c), confirming LRP1 as a major receptor for neuronal uptake of monomeric but not fibrillar tau. Finally, we tested whether synthetic, recombinant fibrillar tau and in vivo AD human brain tau fibrils differ in their use of LRP1 for neuronal entry. To do so, we analysed neuronal uptake of pHrodo-labelled fibrillar tau immunopurified from post-mortem human temporal cortex of individuals who had clinically confirmed sporadic Alzheimer's disease[27]. As with synthetic tau fibrils, inhibiting LRP1 interactions with either RAP or domain IV of LRP1 did not significantly reduce the uptake of postmortem tau aggregates/ filaments,

providing further evidence that tau fibrils do not use LRP1 as a major receptor for neuronal endocytosis.

Monomeric and fibrillar tau enter neurons via distinct endocytosis pathways

To assess the degree of similarity between the mechanisms of neuronal uptake of both forms of tau, we analysed overlaps between the results of both screens at the levels of genes and protein complexes (Fig. 3a,b; Extended Data Fig. 3). To do so, we compared the gene sets identified above from the monomeric and fibrillar tau entry screens, using the $p<0.01$ cutoff. There was a small but significant overlap in a subset of individual genes identified by the screens for monomeric and fibrillar tau uptake (hypergeometric test $p <.001$; Fig. 3a), providing evidence for some shared aspects of neuronal uptake of each form of tau. Genes common to both screens included the COG complex member *COG4*, the three class III PI3K complex members discussed above (*PIK3C3, PIK3R4* and *UVRAG*), and the tyrosine kinase *HGS*, which is a known downstream effector of PI3 kinase, an ESCRT component and regulator of endosome trafficking[28].

In addition to individual genes, genes that contribute to four protein complexes (Fig. 3) were significantly enriched (FDR <0.05) among combined hits of the monomeric and fibrillar tau uptake screens (Fig. 3b). These four were the Conserved Oligomeric Golgi (COG) complex, involved in vesicular trafficking within the Golgi, the vesicular ATPase that acidifies the lysosome and autophagosome, the PIK3 complex discussed above, and the CCC complex, which regulates endosomal recycling, including recycling of receptors[29].

The set of 431 proteins coded by genes significantly enriched in either monomeric or aggregated uptake tau screens were analysed for known direct protein-protein interactions (Extended Data Fig. 2). That analysis generated a network of connected genes that highlights pathways responsible for tau uptake and facilitates identification of densely connected proteins. In agreement with the gene ontology and functional analysis there is a large subnetwork of endosomal and endocytosis proteins, which includes clathrin heavy chain (CLTC), dynamin-2 (DNM2), EEA1 and AP2 subunits. This subnetwork is part of a larger set of interactions that includes RAB7A, LRRK2, PIK3C3 and PIK3R4, all of which have roles in regulating endocytosis and endosome trafficking[20,30]. There are other notable protein interaction subnetworks that regulate vesicle trafficking, endosome sorting, Golgi vesicle trafficking and vacuolar ATPase function. Given that acidification of late endosomes and lysosomes is a key requirement for receptor recycling, disruption of that process is likely to have considerable impact on surface receptor number and composition[31]. Notably, LRRK2 is the most densely connected protein within the protein-protein interaction network. LRRK2

interacts directly with two of the five most connected proteins RAB7A and CLTC. Overall, the number and density of protein-protein interactions in the tau uptake network that mediate endocytosis, endolysosome function and vesicular traffic underscore the importance of receptor-mediated endocytosis for neuronal uptake of extracellular tau.

Predicted tau uptake pathways can be delineated by assigning cellular locations to the proteins coded by genes identified in our tau uptake screens using the COMPARTMENTS dataset (Extended Data Fig. 3). In agreement with the ontology and pathway analyses, monomeric and fibrillar tau show differences in their modes of uptake. Initial interactions between either monomeric or fibrillar tau and the cell surface or plasma membrane require distinct proteins. Once tau enters neurons it is processed by the endolysosomal system, as several proteins required for tau uptake are localised to endosomal, late endosomal and lysosomal compartments. Proteins in the endolysosomal system required for monomeric or fibrillar tau uptake share similarities, including class III phosphatidylinositol 3-kinase (PIK3s) family proteins, but also some notable differences that may reflect distinct processing pathways for forms of tau. Fibrillar tau uptake shows a greater dependency on genes associated with the Golgi apparatus and ER-Golgi trafficking compared with monomeric tau uptake, indicating differences in post-translational modifications required for the uptake of each form of tau.

Uptake of monomeric and fibrillar tau uses different receptors but similar endocytic and intracellular trafficking pathways

The functional genomics screen analyses suggest that, although the early steps of tau endocytosis differ for monomeric and fibrillar tau, including surface receptors, the later stages show considerable convergence. Confirming this, inhibition of dynamin-dependent endocytosis greatly reduced uptake of both monomeric and fibrillar forms of tau (Fig. 4a,b; Extended Data Fig. 4). Similarly, loss of three of the subunits of complex II of class III PI3K all lead to reduced tau uptake, suggesting that class III PI3K activity is required for uptake of all forms of tau, which was confirmed by inhibiting PI3K activity with PIK93 or wortmannin[32] administration before addition of extracellular monomeric or fibrillar tau (Fig. 4a,b).

To test whether disruption of trafficking from the Golgi impacts neuronal ability to endocytose extracellular tau, human iPSC-derived excitatory neurons were treated with Brefeldin A. Live imaging of pHrodo-tau uptake demonstrated reduced uptake of extracellular monomeric and fibrillar tau (Fig. 4c,d; Extended Data Fig. 4), confirming the dependency of tau uptake of both monomeric and fibrillar tau on the integrity of ER-Golgi transport. Finally, tau uptake was assessed in the presence of the autophagy inhibitor bafilomycin A, which targets V-type

ATPase acidification of lysosomes[33]. Human neurons acutely treated with bafilomycin A before the addition of extracellular forms of tau-pHrodo were markedly reduced in pHrodo signal, demonstrating that both forms of tau protein are trafficked via intracellular acid compartments of neurons.

Current models for tau-mediated propagation of pathology between neurons propose pathogenic forms of tau seed aggregation in receiving cells in the cytoplasm. Thus, following endocytosis, extracellular tau is likely to exit the endolysosome as part of its pathogenic mechanism. This echoes the life-cycle of many viruses, which use a variety of mechanisms to enter human cells, including receptor-mediated endocytosis and micropinocytosis[34]. After escaping membrane bound compartments, viral genetic material can be delivered to the cytoplasm or nucleus for replication. The host factors or genes that regulate the entry and life cycle of several viruses have been comprehensively studied using RNAi and CRISPR screens. These include the neurotropic Zika[35], Influenza A[36] and SARS-CoV2[37] viruses, which enter cells via receptor-mediated endocytosis, and Ebola[38], which uses micropinocytosis.

To compare the biology of tau entry and processing with that of genes required for different viruses entry, the sets of genes identified in the screens here were compared with those reported for Influenza A, Zika, SARS-CoV2 and Ebola infection (Fig. 4e). Genes required for the uptake of tau were also compared to genes required for transferrin or epidermal growth factor (EGF) that enter via endocytosis[39] or phagocytosis of beads of different size and charge[40] (Extended Data Fig. 4). Significant overlaps in the number of genes identified in either monomeric and fibrillar tau screens were found with those reported for Influenza A, Zika and SARS-CoV2 infection, but not with Ebola infection (Fig. 4e) or those required for phagocytosis of beads (Extended Data Fig. 4). Monomeric tau uptake shows a small but significant overlap with the endocytosis of transferrin, but there were no other significant overlaps between fibrillar tau uptake, transferrin or EGF endocytosis (Extended Data Fig. 4).

Genes required for both tau entry and either Influenza A, Zika or SARS-CoV2 infection and replication are significantly enriched in genes encoding the vATPase or its assembly, the COG complex and intracellular vesicular trafficking, as reflected in the gene ontology enrichments (Extended Data Fig. 4), with their encoded proteins enriched in proteins localised to the endosome, lysosome and Golgi network (Fig. 4f and Extended Data Fig. 4). The overlap in routes of cell entry by viruses and tau protein, at the levels of both individual genes and cellular pathways, suggests that the cellular factors that regulate tau entry to

neurons are functionally similar to the host factors regulating the intracellular viral life cycle, including cellular entry and access to the cytoplasm.

LRRK2 gain and loss of function mutations disrupt the neuronal endolysosomal system

The large, multidomain protein encoded by *LRRK2* has multiple roles in endocytosis and vesicle trafficking[20] and mutations in *LRRK2* are causal for autosomal dominant PD with neuronal tau aggregation[41,42]. LRRK2 has been found to regulate endolyosomal protein trafficking through its interaction with AP2[43–45]. Mutations in the kinase domain of *LRRK2* or in domains that regulate kinase activity are causal for PD[46]. The most prevalent LRRK2 PD mutation, LRRK2 G2019S[47], stimulates kinase activity[48] and disrupts the endolyosomal system in a variety of transgenic and cell models[20].

We generated cortical neurons from isogenic *LRRK2* wild type, *LRRK2* heterozygous and homozygous null and LRRK2 G2019S iPSCs (Fig. 5a,b; Extended Data Fig. 5). Gene expression analysis confirmed that cultures of each genotype contained excitatory and inhibitory interneurons, with one LRRK2 null and the LRRK2 G2019S mutation iPSCs generating proportionally more interneurons, based on expression of genes indicative of each cell type (Extended Data Fig. 5). Morphological analysis of the endolysosomal system in *LRRK2* mutant neurons found that *LRRK2* homozygous null neurons have clear lysosome enlargement, as previously described in other models[49,50], compared with isogenic controls and LRRK2 heterozygotes, whereas *LRRK2* heterozygous nulls do not have measurable defects (Fig. 5c,d). The endosomal compartments of the LRRK2 null and isogenic control neurons did not show detectable morphological differences (Fig. 5). LRRK2 G2019S mutant neurons showed clear enlargement of early endosome and late endosome/lysosomes, compared with isogenic controls (Fig. 5), as has previously been reported in transgenic LRRK2 G2019S mouse astrocytes[49]. Thus, complete loss of LRRK2 function and kinase-activating mutations in LRRK2 both result in abnormalities of the neuronal endolysosomal system, which are more severe in LRRK2 G2019S neurons than in LRRK2-null neurons, extending to early endosomes (Fig 5e-h).

LRRK2 regulates neuronal endocytosis of monomeric tau, alpha-synuclein and Abeta

To investigate the role of *LRRK2* in neuronal endocytosis of extracellular tau, uptake of extracellular monomeric and fibrillar tau by *LRRK2* heterozygous and homozygous null and *LRRK2* G2019S neurons was analysed by flow cytometry (Fig. 6a,b; Extended Data Fig. 6). *LRRK2* null neurons were significantly reduced in their ability to take up monomeric tau (both wild-type and tau P301S forms), while remaining competent for transferrin uptake (Extended Data Figure 6). Fibrillar tau uptake was not affected by loss of the *LRRK2* gene, confirming

the findings of the primary CRISPR screens (Fig 6c). In contrast, *LRRK2* G2019S neurons demonstrated increased uptake of both monomeric and fibrillar forms of tau (Fig 6; Extended Data Fig. 6).

Given that both loss of LRRK2 function and the kinase-activating LRRK2 G2019S mutation disrupt the endolysosomal system, uptake of additional cargoes relevant to neurodegenerative disease were analysed in the different LRRK2 genotypes (Fig 6d-f). Uptake of monomeric alpha-synuclein, which is also mediated by LRP1[51], was altered in LRRK2 null and G2019S neurons in the same manner as tau, with loss of function reducing uptake, and the G2019S mutation increasing uptake (Fig 6d). Loss of LRRK2 function had no impact on Abeta peptide uptake, whereas the G2019S mutation reduced Abeta uptake (Fig 6e). Finally, receptor-mediated endocytosis of EGF was also reduced by the LRRK2 G2019S mutation, and increased by loss of LRRK2 function (Fig. 6f; Extended Data Figure 6).

Therefore, we conclude that LRRK2 affects the uptake of different cargoes that enter neurons via distinct routes, by regulating multiple endocytic pathways. In particular, tau receptor LRP1-mediated endocytosis pathways are seemingly attenuated by loss of LRRK2 function, as indicated by an accumulation of LRP1 on the cell surface of LRRK2 null neurons (Extended Data Figure 6).

Inhibition of the LRRK2 kinase broadly perturbs receptor-mediated endocytosis

Enhanced LRRK2 kinase activity due to the *LRRK2 G2019S* mutation and reduction in LRRK2 protein levels both dysregulate the neuronal endolysosomal system, but alter tau uptake in different ways. The *LRRK2 G2019S* mutation results in increased uptake of monomeric and fibrillar tau, whereas complete loss of LRRK2 selectively reduces uptake of monomeric, and not fibrillar tau. To further test the dependency of tau uptake on LRRK2 kinase activity, wild-type iPSC-derived neurons were treated with small molecule LRRK2 kinase inhibitors for one week before testing uptake of extracellular monomeric or fibrillar tau (Fig. 7). Following treatment of neurons with LRRK2 selective kinase inhibitors MLi-2[52] and GSK3357679A[53,54], no significant differences in the size of endosomes or lysosomes were detected (Fig. 7a,b; Extended Data Fig. 7). Neuronal uptake of pHrodo-labelled monomeric and fibrillar tau, measured using live-imaging, was reduced after treatment with LRRK2 inhibitors (Fig. 7c,d). Neuronal uptake of transferrin (Alexa 633 conjugate) was not significantly affected by LRRK2 inhibitors (Fig. 7e).

To examine if the apparent LRRK2 kinase inhibition affected neuronal surface levels of LRP1, neurons were treated with MLi-2 or GSK3357679A for one week and surface proteins were labelled with biotin, following the same approach as with the LRRK2 genotypes (Extended Data Fig. 6). Neuronal LRP1 surface levels were increased after treatment with GSK3357679A, compared with vehicle-treated controls. However, this effect was not observed in neurons treated with MLi-2, a difference that may reflect differences in potency between the two inhibitors (Extended Data Fig. 7)[54]. These results highlight the requirement for LRRK2 kinase activity in both monomeric and fibrillar tau uptake, and underscore the differing impacts on tau endocytosis of modulation of LRRK2 kinase activity and reduction or loss of LRRK2 protein.

Discussion

We report here the delineation by whole genome CRISPR knockout screens of the genes required for extracellular tau uptake by human cortical excitatory neurons, the primary cell type affected in tauopathies. Independent screens for full length monomeric and synthetic fibrillar P301S tau avoided making assumptions about the forms and fragments of tau that are present in interstitial fluid in the CNS and of the forms that are competent to enter neurons, providing a broad view of the mechanisms for tau entry to human neurons. Measurement of tau uptake was restricted to analysing the amount of labelled, extracellular tau that was present in neurons hours after uptake, limiting the effect of intracellular degradation of tau. Consistent with our previous findings[9], whole genome screens found that monomeric and fibrillar tau are taken up by neurons by overlapping pathways, with significant differences in the initial steps of endocytosis, most notably the receptors used, the dependency of fibrillar tau uptake on protein glycosylation and the requirement for LRRK2 for monomeric tau endocytosis. The major mode of entry identified in this study for both monomeric and fibrillar tau is endocytosis mediated by different receptors, which is perturbed by a variety of disruptions of the integrity of the endolysosome-autophagy system and intracellular vesicular transport between the Golgi and other cellular compartments.

This study confirmed that the low density lipoprotein receptor LRP1 is a primary receptor for monomeric tau in human neurons, as recently described[11]. The identification of *LRP1* as one of the top two ranked genes required for monomeric tau uptake is an important validation of the functional genomics approach taken here to understanding the cell biology of neuronal tau uptake. It is noteworthy that two different strategies for acutely inhibiting tau-LRP1 interactions, using the RAP chaperone and domain IV of LRP1, confirmed that LRP1 mediates the majority of monomeric tau uptake in neurons, but is not a major receptor for fibrillar tau. This extends to human AD brain fibrillar tau, which we found does efficiently enter human neurons, but does not require interacting with LRP1 to do so.

Although these screens did not identify a single major receptor for fibrillar tau, analogous with LRP1 for monomeric and oligomeric tau, the screens confirmed the established link between heparan sulfate proteoglycans and fibrillar tau uptake[55]. Tau uptake has previously been shown to be mediated by plasma membrane heparan sulfate proteoglycans[55], and mutations in COG complex components result in congenital disorders of glycosylation in humans that have a wide spectrum of neurodevelopmental pathologies[25]. Two genes required for fibrillar tau uptake, *B3GALNT1* and *B3GNTL1,* encode glycosyltransferases[56] and the cell surface proteoglycan, *GPC5*, identified in Alzheimer's disease GWAS[57] is also required for fibrillar tau entry. Thus, it is likely that the loss of COGs and the

glycosyltransferases both result in disruption of cell surface heparan sulfate proteoglycan assembly and thus reduced fibrillar tau uptake.

Beyond the plasma membrane and the initial steps of endocytosis, CRISPR screens for uptake of monomeric and fibrillar tau identified genes and pathways required for uptake of both forms of the protein, but with some differences. Although the specific genes identified in each screen were not identical, there was a high degree of convergence of hits in protein complexes, organelles and cellular pathways. For each form of tau, key regulators of receptor-mediated endocytosis were identified at the level of endocytosis for monomeric tau (clathrin heavy chain and dynamin-2), and within early endosomes for fibrillar tau (EEA1). Beyond the early endosome, tau uptake by human neurons is highly dependent on class III PI3-kinase, which was confirmed by acute small molecule inhibition. Class III PI3K is a major regulator of both endosome recycling to the plasma membrane, as well as autophagy and phagocytosis[30], and its involvement highlights that perturbations of receptor recycling and of wider vesicular trafficking, including autophagy, results in a loss of neuronal capacity for tau uptake. Therefore, we conclude that monomeric/oligomeric and fibrillar tau use different receptors and early endocytic pathways to enter neurons, which then converge in the late endosome/lysosome.

Alterations in receptor recycling are a well-characterised consequence of loss of function of proteins involved in endosome sorting and recycling[31]. We found that loss of components of the CCC complex reduces neuronal uptake of fibrillar and monomeric tau. Sorting nexin-17 (SNX17) is required for monomeric tau uptake, and given that a key cargo for SNX17-mediated recycling is LRP1 and SNX17 interacts with the WASH/CCC complex[21], it is likely that loss of each of these proteins affects plasma membrane levels of LRP1. Similarly, late endosome and lysosome acidification is essential for receptor recycling during the sorting process[58] and we find that loss of multiple vATPase subunits, as well as accessory subunits and assembly proteins, all reduce tau uptake.

The dependency of tau uptake on surface receptor expression, receptor-mediated endocytosis and wider homeostasis of intracellular vesicular trafficking has similarities with the host factors regulating viral entry and replication, particularly for viruses that enter human cells by receptor-mediated endocytosis. Comparing the results of this study with loss of function screens for viral entry, we find significant overlap in genes and protein complexes required in each case. This ranges from endocytosis, through vATPase activity to the COG and TRAPPC complexes in the Golgi. The similarities in the cell biology of the two processes

indicates that tau entry to neurons is a quasi-infectious process, which adapts normal cellular processes to both gain entry to the endolysosome and to propagate within neurons.

We also report here that LRRK2 is required for uptake of monomeric, but not fibrillar tau by human neurons. In contrast, we found that neurons expressing the LRRK2 G2019S, kinase-activating mutation have increased uptake of both extracellular monomeric and fibrillar tau, together with disruption of the endolysosomal system. Consistent with the LRRK2 G2019S gain-of-function data, acute inhibition of the kinase activity of LRRK2 inhibits neuronal uptake of all forms of tau without detectable significant morphological disruption of the endolysomal system, within the detection limits of the number of replicate experiments and imaging systems used here. The role of LRRK2 in endocytosis is not limited to tau, as it also regulates uptake of alpha-synuclein, another LRP1 ligand[51]. The mechanisms by which LRRK2 regulates tau and synuclein endocytosis remain to be elucidated, and may be a direct effect on receptor-mediated endocytosis through LRRK2 interaction with the AP2 clathrin adaptor complex[43–45]. Alternatively, given the widespread changes in the endolysosomal-autophagy system downstream of LRRK2 gain- and loss-of-function[20], LRRK2 may indirectly impact endocytosis of certain cargoes, secondary to perturbation of the endolysosome.

The involvement of LRRK2 and LRP1 in both tau and synuclein uptake by human neurons addresses questions about the role of LRRK2 in tauopathies and the mechanistic links between the pathogenesis of PD and AD and other tauopathies, while opening some new ones. Missense, dominant mutations in *LRRK2* are a cause of familial PD and result in kinase activation, and LRRK2 variants are risk factors for sporadic PD[59]. *LRRK2* mutations causal for genetic PD are commonly accompanied by intraneuronal tau aggregation in the cerebral cortex[46]. Furthermore, missense *MAPT* mutations cause frontotemporal dementia with parkinsonism, and GWAS have identified *MAPT* variants as risk factors for PD[59]. Thus, both *LRRK2* and *MAPT* are associated with the pathogenesis of PD, with *LRRK2* mutations facilitating the development of tau pathology in PD and PD dementia. LRP1 is a receptor for neuronal endocytosis of both tau and alpha-synuclein[11,51], and we report here that LRRK2 regulates endocytosis of both tau and alpha-synuclein by human neurons. Recent GWAS investigating the rate of progression of a tauopathy in progressive supranuclear palsy identified variants in a putative enhancer for *LRRK2* that increase rate of progression, implicating LRRK2 in mediating tauopathy pathogenesis[60]. Together, these findings place LRRK2 together with LRP1 as contributing to tauopathy pathogenesis, and suggest that small molecule inhibition of LRRK2, or reduction in LRRK2 protein levels, may have roles in slowing disease progression in neurodegenerative diseases involving spread of tau

aggregation, including Alzheimer’s disease, as well as PD progression mediated by alpha-synuclein.

Methods

Production and characterization of human iPSC-derived cerebral cortex neurons

Human pluripotent stem cell lines used in this study were KOLF2-C1 (WTSIi018-B-1) and derivative constitutively expressing Cas9 protein (KOLF2-C1 Cas9). KOLF2-C1 Cas9 was generated by integration of a Cas9 transgene driven by a CAG promoter at the AAVS1 locus. Cells were nucleofected (Lonza) with recombinant enhanced specificity Cas9 protein (eSpCas9_1.1)[61], a synthetic crRNA/tracrRNA (target site ggggccactagggacaggattgg) and a homology directed repair template (https://www.addgene.org/86698/) followed by selection in neomycin (50 ug/ml) and clonal isolation[62]. Integrated clones were identified using PCR across the homology arms and validated by Sanger sequencing of the entire transgene and measurements of Cas9 activity. Random integration was screened for using PCR within the antibiotic resistance gene of the template plasmid.

Generation of isogenic gain and loss of function LRRK2 mutation iPSCs.

Optimal gRNA design was performed using the WGE tool (https://wge.stemcell.sanger.ac.uk/) to minimise off target effects. Full length chemically modified sgRNA was purchased (Synthego) with the LRRK2-targeting gRNA sequence: ATTGCAAAGATTGCTGACTA. CRISPR/Cas9 genome editing was performed as previously described[62]. Briefly, eSpCas9_1.1/sgRNA ribonucleoprotein complexes and ssODNs were transfected into iPSCs by electroporation using nucleofection according to the manufacturer's instructions (Lonza 4D nucleofector, CA137, P3 buffer). To generate an isogenic KOLF2 C1 LRRK2 G2019S gain of function iPSC line 500 pmol of a homology directed repair template (sequence: TTTCACACTGTATCCCAATGCTGCCATCATTGCAAAGATTGCTGACTACAGCATTGCTCAGTACTGCTGTAGAATGGGGATAAAAACATCAGAGGGCACAC) was added to the nucleofection. Cells were allowed to grow to 75% confluence, dissociated using Accutase and plated onto a SynthemaxII-SC-coated 10 cm2 dish (Corning) at a low density. Individual colonies were picked manually into 96 well plates coated in matrigel (Thermo Scientific) for expansion and LRRK2 KO clones were identified by high throughput sequencing. Sequencing was performed from PCR products using primers (F-ACACTCTTTCCCTACACGACGCTCTTCCGATCTcagatacctccactcagcca, R-TCGGCATTCCTGCTGAACCGCTCTTCCGATCTtccttttgactcttctgaactca), indexed and sequenced on an Illumina MiSeq instrument, and final clones validated by Sanger sequencing using primers (F-AGGGACAAAGTGAGCACAGAA, R-CACAATGTGATGCTTGCATTTTT).

LRRK2 protein levels from RIPA extracted iPSC lysate were assessed using the AlphaLISA SureFire Ultra Human and Mouse Total LRRK2 Detection Kit (ALSU-TLRRK2-A-HV), excitation emission measurements (615 nm) were corrected with reactions without donor antibody mix and normalised to total protein concentration determined by the Pierce BCA Protein Assay Kit (23227).

Directed differentiation of human iPSCs to cerebral cortex was carried out as described, with minor modifications[18]. To establish cortical identity and quality of neuronal induction, gene expression profiling was performed on a custom gene expression panel[63]. RNA was isolated from iPSC cortical inductions 35 days after induction, using an RNA extraction kit (QIAGEN). Expression of genes in neurons (MAP2, MAPT, and NGN2), cerebral cortex progenitor cells (EMX2, PAX6, and FOXG1), ventral telencephalon (NKX2-1 and LHX8), and mid-/hindbrain (HOXA and HOXB) was assessed in all neuronal inductions on the Nanostring nCounter platform. Immunofluorescent staining was performed on neurons as previously described[64], using the following primary antibodies: tau (Dako, A0024), MAP2 (abcam; ab5392), Tuj1 (Cambridge Bioscience; ab14545), TBR1 (abcam; ab31940), CTIP2 (abcam; ab18465) EEA1 (abcam; ab109110) and LAMP1 (abcam; ab62562). Secondary antibodies used were as follows: anti-mouse Alexa 647 (A32787), anti-rat Alexa 647 (A48265), goat anti-chicken Alexa 488 (A11039), goat anti-rabbit Alexa 546 (A11010, all from Thermo Fisher Scientific). Samples were stained with DAPI (1:5000 in PBS). Images were acquired through Olympus Inverted FV1000 confocal microscope and processed using the Fiji software[65].

Cas9 editing efficiency in human iPSC neurons

Knockout efficiency in KOLF2-C1 Cas9 neurons was assessed using a lentiviral reporter system[15]. Briefly, neurons were transduced (30 days after induction) with lentiviruses expressing fluorophores mCherry and GFP and an sgRNA targeting GFP (pKLV2-U6gRNA(gGFP)-PGKmCherry2AGFP-W; modified from ref. 15. Neurons were dissociated (Accutase [Sigma, A6964]) 5, 12, 17 and 29 days after transduction and analysed by flow cytometry (SH800S Cell Sorter, Sony). Knockout efficiency was calculated as the ratio of mCherry positive, GFP negative neurons over total transduced cells (mCherry positive, GFP positive and negative) (FlowJo software).

Genome-wide CRISPR RNA guide lentiviral library

The Human CRISPR Library v.1.1 was used in this study. The Human CRISPR Libraries v.1.0 and v1.1 have been previously described (Addgene, 67989)[62,66]. CRISPR Library v.1.1 contains all the guides from v1.0 targeting 18,009 genes with 90,709 sgRNAs, plus five additional sgRNAs against 1,876 selected genes[67]. Lentiviruses were produced by

transfecting HEK 293 cells with lentiviral vectors together with packaging vectors (3rd generation) using Lipofectamine 3000 (Thermofisher). Viral supernatant was collected 24hr and 48hr post-transfection, filtered, concentrated by centrifugation and stored at -80°C. The library was sequenced to assess the distribution of the guides. Virus MOI was determined by flow cytometry (SH800S Cell Sorter, Sony; FlowJo software). For each whole-genome CRISPR knockout screen, 4-6×10^7 neurons (35 days after induction) were transduced with an appropriate volume of the lentiviral packaged whole-genome sgRNA library to achieve 30-40% transduction efficiency (>100×library coverage).

Recombinant tau monomer and aggregate preparation

Recombinant tau protein was purified as previously described[9]. Briefly, tau P301S_FLAG×3_10×his-tag was overexpressed using the pET24d plasmid in BL21(DE3) bacteria (37°C, 50mg.mL^{-1} Kanamycin, IPTG 0.4mM). Cells were lysed (Avestin Emulsiflex C5) in lysis/binding buffer (20mM phosphate [pH7.4], 500mM NaCl, 20mM imidazole, protease inhibitor cocktail [Roche]), clarified lysate was applied to a 5mL HisTrapHP column (GE Healthcare) and washed with 10CV of lysis/binding buffer. Tau was eluted in 20mM phosphate (pH7.4), 500mM NaCl, 500mM imidazole. Peak fractions were pooled and further purified using a Superdex 200 16/60 gel filtration column (GE Healthcare) in 50mM phosphate (pH7.4), 150mM NaCl. Pooled fractions were then concentrated to approximately 8 mg/mL using a spin concentrator (Millipore). Tau fibrils were prepared following the protocol and characterisation as described[9]. 1mL tau P301S at 8mg/mL was incubated with 4 mg.mL^{-1} heparin (Sigma) in PBS plus 30 mM 3-(N-morpholino)propanesulfonic acid (MOPS) (pH 7.2) at 37°C for 72 hr. fibrillar material was diluted in 9 mL PBS plus 1% (v/v) sarkosyl (Sigma) and left rocking for 1 hr at room temperature to completely solubilize any non-fibrillar material. Insoluble tau was pelleted by ultracentrifugation for 1hr at 4°C. The pellet was resuspended in 1mL PBS by vigorous pipetting and sonicated at 100W for 3×20s (Hielscher UP200St ultrasonicator) to disperse clumps of protein and break large filaments into smaller species. Final protein concentration was determined by the Pierce BCA Protein Assay Kit (23227).

To label purified recombinant tau (monomeric or fibrillar tau P301S) with Dylight 488 NHS ester (Thermo Fisher Scientific) or pH-sensitive form of rhodamine (pHrodo, Thermo Fisher Scientific), 150 μM tau protein (or equivalent protein concentration for aggregate; ~7 μg.mL^{-1}) was incubated with either a 10 fold-molar excess of Dylight (10mg.mL^{-1}; dissolved in DMF) or pHrodo (10mM; dissolved in DMSO; with 10 fold molar excess of tris[2-carboxyethyl]phosphine; TCEP) for 2hrs in the dark at room temperature. After incubation,

labelled protein samples were subjected to size exclusion chromatography at 4°C (Superdex 200 Increase 10/300 GL, GE Healthcare) in 50 mM phosphate (pH 7.4) and 150 mM NaCl to remove unreacted dye and assess perturbation of oligomeric state by labelling (no change was observed, data not shown). 64.5μM Transferrin from Human Serum, Alexa Fluor™ 633 Conjugate **(**T23362; Thermo Fisher Scientific) was dissolved in PBS.

Flow cytometry-based whole-genome screen for genes modifying tau entry and processing
Neurons transduced with the Human CRISPR library were matured in neuronal maintenance medium (N2B27; media changed every two days) for 65 days. 24hrs prior to acute incubation with labelled recombinant proteins, media was exchanged to DMEM plus supplements (500ml DMEM/F-12 + GlutaMAX, 0.25mL Insulin (4mg.mL^{-1}), 1mL 2-Mercaptoethanol (50mM), 5mL MEM Non-Essential Amino Acids Solution, 5mL Sodium pyruvate (100mM) and 2.5mL Penicillin-Streptomycin (10,000 U/mL); ThermoFisher; note this is without N2 supplement that contains transferrin) to remove transferrin from the culture medium. The following day neurons were incubated with 30nM of transferrin-Alexa 633 and either 90nM monomeric or 400nM fibrillar tau-Dylight for 4 or 5hrs, respectively. After two PBS washes, neuronal cultures were dissociated with papain (Worthington biochemical Corporation) supplemented with Accutase (Sigma, A6964) into single cells.

Dissociated neurons were collected by low-speed centrifugation (600×*g* for 15min), the supernatant was removed, filtered (Sysmex/Partec CellTrics 50μm filter) and fixed using 2% paraformaldehyde in PBS for 15min at room temperature. Neurons were washed twice in PBS, resuspended in PBS, 7.5% w/v BSA, 2mM EDTA and analysed by flow cytometry. Flow cytometry assays were performed on a Sony SH800 Cell Sorter or BD LSRFortessa Cell. For large scale CRISPR knockout screens neurons were collected using a BD Influx cell sorter. Neurons were gated using forward and side scatter channels to isolate the viable cell population and exclude noise/debris, subsequently gated on forward scatter and trigger pulse width channel to isolate singlets. MAP2 positive cells were identified using Milli-Mark Anti-MAP2-PE antibody (Sigma-Aldridge; FCMAB318PE). Transferrin and tau uptake assays were gated for fluorescence in the channels corresponding to BFP (sgRNA library), Dylight 488 (tau) and Alexa 633 (transferrin), using non transduced neurons and neurons without acute incubation of recombinant proteins to establish thresholds. Neuronal populations were collected that were positive for the sgRNA library and had high levels of labelled transferrin and either high or low levels of labelled tau protein.

Guide RNA sequencing

Genomic DNA was extracted from cell pellets using QuickExtract DNA Extraction Solution (Cambio; QE09050) as per the manufacturer's instructions. sgRNA amplification was performed using a two-step PCR strategy and purified using Agencourt AMPure XP (A63880; Beckman Coulter UK), Illumina sequencing (19-bp single-end sequencing with custom primers on the HiSeq2500 Rapid Run) and sgRNA counting were performed as described previously[15].

CRISPR screen data analysis

sgRNA count files from purified neuronal populations that had high levels of labelled transferrin and tau were compared to neuronal populations with high levels of labelled transferrin and low levels of labelled tau protein using MAGeCK (0.5.8)[19]. Data from replicate monomeric (n=2) or fibrillar (n=3) tau uptake screens were grouped in the analysis. sg-RNA rankings were summarised into gene-level statistics using the RRA algorithm. All subsequent analyses were performed in RStudio (Version 1.3.1093). For genes with two sets of sgRNAs, the higher ranking set was kept and the lower ranking set was discarded. An empirical threshold of unadjusted p-value < 0.01 was used to identify genes required for tau uptake in either screen, identifying 214 genes in the fibrillar screen and 228 genes in the monomeric screen. Functional term enrichment analysis was performed using gProfiler 2 querying the GO, REAC, and CORUM databases[68], for the term enrichment analysis individual gene names from the library were manually updated to their most current name as indicated in Supplementary Table 2.

Compartment localisation enrichment was performed using localisation scores from the COMPARTMENTS database[69]. Localisation of each gene to a particular compartment is given a score up to 5 based on the strength of the supporting evidence. To calculate compartment localisation enrichment for the genes identified in the CRISPR screens, a gene set localisation score for each compartment was calculated by averaging the localisation score of all constitutive genes. The score ranged from 0 to 1, with 1 representing maximum localisation score for that compartment for all the genes in the set. Cellular compartments were removed from analysis if too undescriptive (gene-set localisation score >= 0.7), with low signal (gene-set localisation score <= 0.02), or with only weak evidence (no individual gene scoring 3.5/5 or above). Compartment localisation enrichment was calculated compared to the mean value obtained from 100,000 simulated random sets of 228 (fibrillar), 214 (monomeric), 431 (combined fibrillar and monomeric), or 21 (combined fibrillar and monomeric, and either Zika, InfluenzaA, or Coronavirus) genes from the CRISPR library. Boot-strapping was used to calculate p-values and significance was adjusted for multiple comparison using false discovery rate. For significantly enriched compartments, the log2

fold-change of compartment score over random set average was mapped onto a diagram of cellular compartments using the sp package[70].

Protein-protein interaction networks were constructed using the PSICQUIC package using the following databases: BioGrid, bhf-ucl, IntAct, MINT, UniProt, MBInfo, InnateDB [71]. All PPIs for the human proteins were maintained, removing reciprocal and self-interactions. Network graphs were drawn using igraph and visNetwork packages [72].

Flow cytometry analysis of extracellular protein uptake in neurons with individual gene perturbations

KOLF2-C1 Cas9 neurons were transduced with lentiviruses (30 days after induction) containing vectors expressing CRISPR-Cas9 guides targeting individual genes (Supplementary Table 4), pKLV2-U6gRNA5(BbsI)-ccdb-PGKpuro2ABFP-W (modified from Addgene, 67974). Transduced or CRISPR engineered (LRRK2 gain and loss of function mutations) neurons were maintained (65 days) and subsequently assayed for their ability to take up recombinant extracellular protein as previously described with modifications to protein concentrations and incubation times. Neurons were incubated with 90nM of transferrin-Alexa 633 and either 90nM monomeric (wild-type or P301S; 4hr incubation), 400nM fibrillar tau-Dylight 488 (5hr incubation), β-amyloid (1-42) HiLyte™ Fluor 488 (5hr incubation; Anaspec; AS-60479-01), 100nM α-synuclein (1-140), HiLyte™ Fluor 488 labelled (5hr incubation; Anaspec; AS-55457), 150nM epidermal Growth Factor, Fluorescein Conjugate (3hr incubation; Thermo Fisher Scientific; E3478), or 500nM Dextran, Fluorescein, 70,000 MW, (3hr incubation; Thermo Fisher Scientific; D1823). Dissociated neurons were analysed by flow cytometry (BD Fortessa Cell Analyzer). For LRRK2 G2019S neurons, uptake of tau was measured in independent experiments at two sites (Sanger Institute and Babraham Institute, Cambridge), using two different FACS platforms (BD Fortessa and ThermoFisher Attune CytPix). Gated singlet neurons were assessed for fluorescence in the channels corresponding to the labelled proteins above, thresholds were established as described previously. Flow cytometry data were analysed using FlowJo software.

Live imaging of tau entry to human iPSC neurons

Neurons grown (65 days after induction) on 96-well plates (CellCarrier96; Perkin Elmer Life Sciences; 6055308) were imaged for fluorescent pHrodo-labelled tau protein (excitation at 577nm and emission at 641nm in an acidic environment) using a Opera-Phenix (Perkin Elmer). Bright-field and fluorescence emission images were collected at 45min or 1hr intervals for between four and ten hours at 37°C, 5% CO_2. Parameters for fluorescent

objects were set (fluorescent intensity and contrast), quantified and intensity of the field was normalised to confluency using the Incucyte Analysis Software. Data was analysed using Prism Software (GraphPad). Typically, conditions were repeated at least in triplicate and nine fields recorded per well.

Live imaging assays were performed using monomeric (50nM) or fibrillar (100nM, equivalent calculated from monomeric tau; 5ug.mL^{-1}) pHrodo-labelled tau. For competitive binding experiments, recombinant peptides were resuspended in PBS, and PBS was the vehicle control in experiments. Recombinant proteins were separately preincubated with neuronal cultures and recombinant tau protein for 3 hours prior to incubation of neuronal cultures with the mixer containing recombinant proteins (100nM Human LRP-1 Cluster IV Fc Chimera Protein; 10nM Human LRPAP Protein [R&D systems]). For pharmacological treatments, compounds were dissolved in DMSO at the concentrations noted, and DMSO was the vehicle control in experiments. A one week pharmacological treatment regime of neurons, exchanging media every 48 hours, was employed for Dynasore (2897), PIK93 (6440), wortmannin (1232), MLi-2 (5756; Tocris Bioscience), GSK3357679A (GSK) or vehicle control (0.1% [v/v] DMSO). A 24 hour treatment regime of neurons was employed for Brefeldin (1231), Bafilomycin (1334; Tocris Bioscience) or vehicle control (0.1% [v/v] DMSO). Neurotoxicity/neurolysis were assessed by analysing the level of lactate dehydrogenase (LDH) activity (Roche; 11644739001) in conditioned media samples following treatments.

Determination of relative surface protein levels

Neurons grown (65 days after induction) on 24-well plates (Nunc 24-Well Plate, Round, 144530). Following steps were carried out on ice. Neurons were washed three times with 0.5 mL Dulbecco's phosphate-buffered saline (DPBS) with calcium and magnesium (CM-PBS, 14040133; ThermoFisher Scientific). Neurons were then incubated with biotin buffer (0.2 mg.ml-1 EZlink sulfo-NHS-SS-biotin, 21331, ThermoFisher Scientific in CM-PBS) for 30 minutes followed by replacement of Biotin buffer with quenching reagent (50 mM NH4Cl in CM-PBS) and left for 10 minutes. Following a repeat of the quenching step and three subsequent washes in CM-PBS, neurons were resuspended in RIPA buffer (thermo) containing cOmplete Protease Inhibitor Cocktail (Roche; 11697498001) and transferred to 0.5 mL Soft tissue homogenising CK14 tubes (Bertin) and lysed using the Precellys Evolution system. Neuronal lysates were left for 5 minutes and centrifuged at 16,000×g for 10 minutes. The protein concentration of isolated lysate supernatant measured using the Pierce BCA Protein Assay Kit (23227). Normalised protein lysates (cell lysate) were incubated overnight with 40µL (50% slurry) of SpeedBeads Magnetic Neutravidin Coated

particles (GE78152104010150) on a rotator. Surface biotinylated proteins bound to Neutravidin beads were separated from unlabelled intracellular proteins by magnetism, washed four times in 1mL of wash buffer (10 mM Tris (pH 7.4), 1.5 mM EDTA, 150 mM NaCl, 1% Triton X-100, containing cOmplete Protease Inhibitor Cocktail). After centrifugation at 1,500×g for 30 seconds and removal of residual wash buffer, surface proteins bound to beads were resuspended in 50uL of NuPAGE™ LDS Sample Buffer (NP0007) and denatured at 95°C for 10 minutes. Resulting samples (cell lysate and surface fractions) were analysed by western blot using antibodies for LRP1 (Abcam; ab92544; 1:1000), N Cadherin (ab18203) and β-Actin (Sigma-Aldrich; A2228; 1:1000). Primary antibodies were used at 1:1000 dilution and incubated overnight in PBS with 3% (w/v) Bovine Serum Albumin (Sigma-Aldrich; A3983), and detected using secondary IgG antibodies conjugated to fluorescent probes (Alexa Fluor 488; A-2120; Alexa Fluor 546; A10040). Protein levels were assessed using a ChemiDoc Imaging System and the Image lab software (BioRad).

Statistical Analysis

The number of replica wells and experiments are indicated in the figure legends for each assay where appropriate. For live-cell imaging assays using pHrodo-labeled protein, intensity was normalised to area of the field occupied by cells using the Incucyte Analysis Software. Typically, 9 fields were recorded per well and an average generated from the Incucyte Analysis Software. Analyses were performed using the Prism version 8 software (GraphPad). One-way ANOVA with Dunnett's multiple testing or Student's t test was used where appropriate.

Hypergeometric tests were used to evaluate significance of overlap between gene sets. Genes required for uptake of Ebola, influenza A, Zika and SARS-CoV2 viruses, and for different size beads were obtained from published CRISPR screens [35, 36, 38] and were defined as having an FDR < 0.05. Genes required for uptake of transferrin and EGF were obtained from a published RNAi screen[39] and defined as having $\chi 2$ probability $(1.0 - P) \geq 0.95$. Hypergeometric tests for overlap in screen hits were carried out using the set of genes analysed in both studies as background.

Acknowledgements

The authors thank Sarah Spain, Paris Litterick, Alison Mann, Gosia Trynka, David Hulcoop and Ian Dunham of the Open Targets team at the European Bioinformatics Institute and Wellcome Sanger Institute for ongoing support of this research; Fiona Behan, Chun-Fang Xu (GSK) and Jinkuk Choi (Biogen) for feedback on data interpretation; Sam Thompson, Jennie

Graham, Chris Hall and Bee Ling Ng for flow cytometry support, Kathleen Long and Michaela Bruntraeger who generated iPSC cell lines (Sanger Institute); Tom Campbell, Sergey Sitnikov and Clare Jones for technical assistance (Talisman Therapeutics) and Anne Hedegaard (University of Oxford) for providing reagents.

Funding

This work was funded by Open Targets (OTAR036, www.opentargets.org). This research was also supported by Wellcome (Investigator Award to FJL), Alzheimer's Research UK (Stem Cell Research Centre), Dementias Platform UK (Stem Cell Network) and Great Ormond Street Hospital Charity. This research was supported in part by the NIHR Great Ormond Street Hospital Biomedical Research Centre. The views expressed are those of the author(s) and not necessarily those of the NHS, the NIHR, or the Department of Health.

Competing interests

Open Targets is a public–private partnership between non-profit research institutions and the pharmaceutical industry. FJL is a founder and holds equity in Gen2 Neuroscience and Talisman Therapeutics.

References

1. Lee, V. M.-Y., Goedert, M. & Trojanowski, J. Q. Neurodegenerative Tauopathies. *Annual Review of Neuroscience* **24**, 1121–1159 (2001).
2. Goedert, M., Eisenberg, D. S. & Crowther, R. A. Propagation of Tau Aggregates and Neurodegeneration. *Annu. Rev. Neurosci.* **40**, 189–210 (2017).
3. Braak, H. & Braak, E. Neuropathological stageing of Alzheimer-related changes. *Acta Neuropathol.* **82**, 239–259 (1991).
4. Vogel, J. W. *et al.* Spread of pathological tau proteins through communicating neurons in human Alzheimer's disease. *Nature Communications* **11**, 2612 (2020).
5. Asai, H. *et al.* Depletion of microglia and inhibition of exosome synthesis halt tau propagation. *Nat Neurosci* **18**, 1584–1593 (2015).
6. Kaniyappan, S. *et al.* FRET-based Tau seeding assay does not represent prion-like templated assembly of Tau fibers. *bioRxiv* 2020.03.25.998831 (2020) doi:10.1101/2020.03.25.998831.
7. Walsh, D. M. & Selkoe, D. J. A critical appraisal of the pathogenic protein spread hypothesis of neurodegeneration. *Nat Rev Neurosci* **17**, 251–260 (2016).
8. Holmes, B. B. *et al.* Heparan sulfate proteoglycans mediate internalization and propagation of specific proteopathic seeds. *Proc Natl Acad Sci U S A* **110**, E3138-3147 (2013).
9. Evans, L. D. *et al.* Extracellular Monomeric and Aggregated Tau Efficiently Enter Human Neurons through Overlapping but Distinct Pathways. *Cell Rep* **22**, 3612–3624 (2018).
10. Rauch, J. N. *et al.* Tau Internalization is Regulated by 6-O Sulfation on Heparan Sulfate Proteoglycans (HSPGs). *Scientific Reports* **8**, 6382 (2018).
11. Rauch, J. N. *et al.* LRP1 is a master regulator of tau uptake and spread. *Nature* **580**, 381–385 (2020).
12. Clavaguera, F. *et al.* Transmission and spreading of tauopathy in transgenic mouse brain. *Nat Cell Biol* **11**, 909–913 (2009).
13. Frost, B., Jacks, R. L. & Diamond, M. I. Propagation of tau misfolding from the outside to the inside of a cell. *J Biol Chem* **284**, 12845–12852 (2009).
14. Sato, C. *et al.* Tau Kinetics in Neurons and the Human Central Nervous System. *Neuron* **97**, 1284-1298.e7 (2018).
15. Tzelepis, K. *et al.* A CRISPR Dropout Screen Identifies Genetic Vulnerabilities and Therapeutic Targets in Acute Myeloid Leukemia. *Cell Rep* **17**, 1193–1205 (2016).
16. McEwan, W. A. *et al.* Cytosolic Fc receptor TRIM21 inhibits seeded tau aggregation. *Proc Natl Acad Sci U S A* **114**, 574–579 (2017).
17. Shi, Y., Kirwan, P., Smith, J., Robinson, H. P. C. & Livesey, F. J. Human cerebral cortex development from pluripotent stem cells to functional excitatory synapses. *Nat. Neurosci.* **15**, 477–486, S1 (2012).
18. Shi, Y., Kirwan, P. & Livesey, F. J. Directed differentiation of human pluripotent stem cells to cerebral cortex neurons and neural networks. *Nat Protoc* **7**, 1836–1846 (2012).
19. Li, W. *et al.* MAGeCK enables robust identification of essential genes from genome-scale CRISPR/Cas9 knockout screens. *Genome Biol.* **15**, 554 (2014).
20. Taylor, M. & Alessi, D. R. Advances in elucidating the function of leucine-rich repeat protein kinase-2 in normal cells and Parkinson's disease. *Current Opinion in Cell Biology* **63**, 102–113 (2020).
21. McNally, K. E. *et al.* Retriever is a multiprotein complex for retromer-independent endosomal cargo recycling. *Nat. Cell Biol.* **19**, 1214–1225 (2017).

22. Hoshi, T. *et al.* Mesdc2 plays a key role in cell-surface expression of Lrp4 and postsynaptic specialization in myotubes. *FEBS Lett.* **587**, 3749–3754 (2013).
23. Hill, K. J. & Stevens, T. H. Vma21p is a yeast membrane protein retained in the endoplasmic reticulum by a di-lysine motif and is required for the assembly of the vacuolar H(+)-ATPase complex. *Mol. Biol. Cell* **5**, 1039–1050 (1994).
24. Liang, C., Feng, P., Ku, B., Oh, B.-H. & Jung, J. U. UVRAG: a new player in autophagy and tumor cell growth. *Autophagy* **3**, 69–71 (2007).
25. D'Souza, Z., Taher, F. S. & Lupashin, V. V. Golgi inCOGnito: From vesicle tethering to human disease. *Biochim Biophys Acta Gen Subj* 129694 (2020) doi:10.1016/j.bbagen.2020.129694.
26. Herz, J., Goldstein, J. L., Strickland, D. K., Ho, Y. K. & Brown, M. S. 39-kDa protein modulates binding of ligands to low density lipoprotein receptor-related protein/alpha 2-macroglobulin receptor. *J. Biol. Chem.* **266**, 21232–21238 (1991).
27. Falcon, B. *et al.* Tau filaments from multiple cases of sporadic and inherited Alzheimer's disease adopt a common fold. *Acta Neuropathol* **136**, 699–708 (2018).
28. Raiborg, C. & Stenmark, H. The ESCRT machinery in endosomal sorting of ubiquitylated membrane proteins. *Nature* **458**, 445–452 (2009).
29. Bartuzi, P. *et al.* CCC- and WASH-mediated endosomal sorting of LDLR is required for normal clearance of circulating LDL. *Nat Commun* **7**, 10961 (2016).
30. Bilanges, B., Posor, Y. & Vanhaesebroeck, B. PI3K isoforms in cell signalling and vesicle trafficking. *Nature Reviews Molecular Cell Biology* **20**, 515–534 (2019).
31. Cullen, P. J. & Steinberg, F. To degrade or not to degrade: mechanisms and significance of endocytic recycling. *Nat. Rev. Mol. Cell Biol.* **19**, 679–696 (2018).
32. Cuenda, A. & Alessi, D. R. Use of kinase inhibitors to dissect signaling pathways. *Methods Mol. Biol.* **99**, 161–175 (2000).
33. Bowman, E. J., Siebers, A. & Altendorf, K. Bafilomycins: a class of inhibitors of membrane ATPases from microorganisms, animal cells, and plant cells. *Proc Natl Acad Sci U S A* **85**, 7972–7976 (1988).
34. Thorley, J. A., McKeating, J. A. & Rappoport, J. Z. Mechanisms of viral entry: sneaking in the front door. *Protoplasma* **244**, 15 (2010).
35. Li, Y. *et al.* Genome-wide CRISPR screen for Zika virus resistance in human neural cells. *Proc. Natl. Acad. Sci. U.S.A.* **116**, 9527–9532 (2019).
36. Li, B. *et al.* Genome-wide CRISPR screen identifies host dependency factors for influenza A virus infection. *Nat Commun* **11**, 164 (2020).
37. Z, D. *et al.* Identification of Required Host Factors for SARS-CoV-2 Infection in Human Cells. *Cell* **184**, (2021).
38. Flint, M. *et al.* A genome-wide CRISPR screen identifies N-acetylglucosamine-1-phosphate transferase as a potential antiviral target for Ebola virus. *Nat Commun* **10**, 285 (2019).
39. Collinet, C. *et al.* Systems survey of endocytosis by multiparametric image analysis. *Nature* **464**, 243–249 (2010).
40. Haney, M. S. *et al.* Identification of phagocytosis regulators using magnetic genome-wide CRISPR screens. *Nat Genet* **50**, 1716–1727 (2018).
41. Rajput, A. *et al.* Parkinsonism, Lrrk2 G2019S, and tau neuropathology. *Neurology* **67**, 1506–1508 (2006).
42. Poulopoulos, M. *et al.* Clinical and pathological characteristics of LRRK2 G2019S patients with PD. *J Mol Neurosci* **47**, 139–143 (2012).

43. Roosen, D. A. & Cookson, M. R. LRRK2 at the interface of autophagosomes, endosomes and lysosomes. *Mol Neurodegener* **11**, 73 (2016).
44. Heaton, G. R. *et al.* Sequential screening nominates the Parkinson's disease associated kinase LRRK2 as a regulator of Clathrin-mediated endocytosis. *Neurobiol. Dis.* **141**, 104948 (2020).
45. Liu, Q., Bautista-Gomez, J., Higgins, D. A., Yu, J. & Xiong, Y. Dysregulation of the AP2M1 phosphorylation cycle by LRRK2 impairs endocytosis and leads to dopaminergic neurodegeneration. *Sci Signal* **14**, eabg3555 (2021).
46. Henderson, M. X., Sengupta, M., Trojanowski, J. Q. & Lee, V. M. Y. Alzheimer's disease tau is a prominent pathology in LRRK2 Parkinson's disease. *acta neuropathol commun* **7**, 183 (2019).
47. Gilks, W. P. *et al.* A common LRRK2 mutation in idiopathic Parkinson's disease. *Lancet* **365**, 415–416 (2005).
48. West, A. B. *et al.* Parkinson's disease-associated mutations in leucine-rich repeat kinase 2 augment kinase activity. *Proc. Natl. Acad. Sci. U.S.A.* **102**, 16842–16847 (2005).
49. Henry, A. G. *et al.* Pathogenic LRRK2 mutations, through increased kinase activity, produce enlarged lysosomes with reduced degradative capacity and increase ATP13A2 expression. *Hum Mol Genet* **24**, 6013–6028 (2015).
50. Pellegrini, L. *et al.* Proteomic analysis reveals co-ordinated alterations in protein synthesis and degradation pathways in LRRK2 knockout mice. *Hum Mol Genet* **27**, 3257–3271 (2018).
51. Chen, K. *et al.* LRP1 is a neuronal receptor for α-synuclein uptake and spread. *Molecular Neurodegeneration* **17**, 57 (2022).
52. Fell, M. J. *et al.* MLi-2, a Potent, Selective, and Centrally Active Compound for Exploring the Therapeutic Potential and Safety of LRRK2 Kinase Inhibition. *J Pharmacol Exp Ther* **355**, 397–409 (2015).
53. Singh, F. *et al.* Pharmacological rescue of impaired mitophagy in Parkinson's disease-related LRRK2 G2019S knock-in mice. *Elife* **10**, e67604 (2021).
54. Tasegian, A., Singh, F., Ganley, I. G., Reith, A. D. & Alessi, D. R. Impact of Type II LRRK2 inhibitors on signaling and mitophagy. *Biochem J* **478**, 3555–3573 (2021).
55. Holmes, B. B. *et al.* Proteopathic tau seeding predicts tauopathy in vivo. *PNAS* **111**, E4376–E4385 (2014).
56. Ricci Hagman, J., Westman, J. S., Hellberg, Å. & Olsson, M. L. An update on the GLOB blood group system (and former GLOB collection). *Immunohematology* **34**, 161–163 (2018).
57. Wang, H. *et al.* Genome-wide interaction analysis of pathological hallmarks in Alzheimer's disease. *Neurobiol Aging* **93**, 61–68 (2020).
58. McNally, K. E. & Cullen, P. J. Endosomal Retrieval of Cargo: Retromer Is Not Alone. *Trends Cell Biol.* **28**, 807–822 (2018).
59. Hardy, J. Genetic analysis of pathways to Parkinson disease. *Neuron* **68**, 201–206 (2010).
60. Jabbari, E. *et al.* Genetic determinants of survival in progressive supranuclear palsy: a genome-wide association study. *Lancet Neurol* **20**, 107–116 (2021).
61. Slaymaker, I. M. *et al.* Rationally engineered Cas9 nucleases with improved specificity. *Science* **351**, 84–88 (2016).
62. Bruntraeger, M., Byrne, M., Long, K. & Bassett, A. R. Editing the Genome of Human Induced Pluripotent Stem Cells Using CRISPR/Cas9 Ribonucleoprotein Complexes. *Methods Mol. Biol.* **1961**, 153–183 (2019).

63. Strano, A., Tuck, E., Stubbs, V. E. & Livesey, F. J. Variable Outcomes in Neural Differentiation of Human PSCs Arise from Intrinsic Differences in Developmental Signaling Pathways. *Cell Rep* **31**, 107732 (2020).
64. Moore, S. *et al.* APP metabolism regulates tau proteostasis in human cerebral cortex neurons. *Cell Rep* **11**, 689–696 (2015).
65. J, S. *et al.* Fiji: an open-source platform for biological-image analysis. *Nature methods* vol. 9 https://pubmed.ncbi.nlm.nih.gov/22743772/ (2012).
66. Behan, F. M. *et al.* Prioritization of cancer therapeutic targets using CRISPR-Cas9 screens. *Nature* **568**, 511–516 (2019).
67. Wang, T., Wei, J. J., Sabatini, D. M. & Lander, E. S. Genetic screens in human cells using the CRISPR-Cas9 system. *Science* **343**, 80–84 (2014).
68. Raudvere, U. *et al.* g:Profiler: a web server for functional enrichment analysis and conversions of gene lists (2019 update). *Nucleic Acids Res* **47**, W191–W198 (2019).
69. Binder, J.X., et al., *COMPARTMENTS: unification and visualization of protein subcellular localization evidence.* Database (Oxford), 2014. **2014**: p. bau012.
70. Bivand, R., E.J. Pebesma, and V. Gómez-Rubio, *Applied spatial data analysis with R*. Second edition. ed. Use R! 2013, New York: Springer. xviii, 405 pages.
71. Aranda, B., et al., *PSICQUIC and PSISCORE: accessing and scoring molecular interactions.* Nat Methods, 2011. **8**(7): p. 528-9.
72. Almende B. V., T.B., Robert, T. , *visNetwork: Network Visualization using 'vis.js' Library. R package version 2.0.9.* 2021: http://datastorm-open.github.io/visNetwork/.

Figure Legends

Fig. 1. FACS-based CRISPR knockout screens in human neurons to identify genes and pathways required for uptake of extracellular tau

(A) Design of whole-genome CRISPR knockout screens for uptake of tau by human iPSC-derived neurons. (B) Representative confocal microscopy images confirming the cortical, excitatory identity of differentiated human (KOLF2-C1) iPSC-derived neurons, constitutively expressing Cas9 protein and the isogenic control. Upper panels, neurons immunolabelled for TUJ1 (neuron-specific β3-tubulin; red), MAP2 (neuronal dendrites; green), TBR1 (deep layer neurons; magenta) and DAPI (nuclear DNA; blue). Lower panels, neurons immunolabelled for MAPT (tau protein; red), MAP2 (green), CTIP2 (deep layer neurons; magenta) and DAPI (blue). Scale bar, 50μm. (C) iPSC-derived cortical neural progenitor cells and neurons retain Cas9 activity after differentiation. Scatterplot of FACS measuring Cas9 activity using a lentiviral Cas9-activity reporter, expressing mCherry and GFP. Left panel, iPSC-derived neurons (parental control line) transduced with lentiviral reporter but not expressing Cas9, middle panel neurons expressing Cas9 without lentiviral reporter and right panel neurons expressing Cas9 with lentiviral reporter. (D) FACS analysis of the percentage of GFP gene-edited neurons against days after reporter infection, measured using the reporter system described in C. (E,F) Transferrin does not compete with or alter extracellular tau uptake by human excitatory neurons. Human iPSC-derived neurons were incubated with monomeric (E; purple) or fibrillar (F; orange) tau protein (Dylight 488 labelled) and transferrin (Alexa 633 conjugate; concentrations indicated) and analysed by flow cytometry. Neurons without tau or transferrin incubation (light blue) were used to establish the threshold level for detection of tau-Dylight fluorescence. Percentage of monomeric or fibrillar tau positive neurons at indicated transferrin concentrations plotted over time after protein incubation initiation. (G) Representative scatter plot of FACS analysis of population of neurons from typical screen outcome, highlighting neurons expressing gRNAs (gated on BFP signal) that are tau-negative but transferrin-positive (dashed red line) and tau-positive and transferrin-positive (dashed black line). See also Extended Data Fig. 1.

Fig. 2. CRISPR loss of function screens identify genes and pathways required for human neuronal uptake of extracellular monomeric and fibrillar tau

Genes required for uptake of tau into human iPSC-derived excitatory neurons identified by comparing FACS collected populations of CRISPR edited neurons, positive for labelled transferrin, but not tau protein against neurons positive for both labelled proteins. Whole-genome enrichment score (-log10 positive score) is plotted against the positive enrichment ranking from the knockout screens for tau uptake derived using MAGeCK algorithm. Applying a p-value cut-off of 0.01, 214 genes were identified as required for (A) monomeric tau uptake (purple points; 2 repeats) and 228 genes were identified as required for (C) fibrillar tau uptake (orange points; 3 repeats). The 10 highest scoring genes are labelled. Heat maps showing a representative selection of significantly enriched terms annotating the genes required for (B) monomeric and (D) fibrillar tau uptake. Grayscale indicates significance level (-log10 FDR). Rows are sorted in order of significance, see Supplementary Table 2 for ranked genes required for tau uptake ($p<0.01$). Each heatmap shows which of the enriched genes is annotated with each term (Supplementary Table 3).

(E) Scatter plot of FACS analysis of monomeric tau and transferrin uptake by iPSC-neurons individually targeted for CRISPR knockout of AP2M1 or non-targeting control (GFP).

(F) Validation of genes identified in primary screens as required for monomeric tau uptake. The percentage of low tau neurons (tau-/transferrin+) is expressed as fold change from the non-targeting control (GFP). Two independent experiments are represented by circles and triangles (Supplementary Table 4).

(G-I) Entry of monomeric tau into neurons is mediated by LRP1, inhibited by addition of extracellular RAP chaperone or LRP1 domain IV peptide. The number of tau positive objects detected over 4 hr by time-lapse imaging of iPSC-derived human excitatory neurons was used to assess neuronal uptake of monomeric (A), fibrillar (B) or post-mortem AD brain (C) tau-pHrodo. Object measurements are displayed over time. 24 independent measurements were taken from at least three technical replicates at 45-minute intervals.

See also Extended Data Fig. 2.

Fig. 3. Uptake mechanisms of monomeric and fibrillar tau differ at the neuronal surface but share intracellular trafficking pathways.

(A) Monomeric and fibrillar tau share common intracellular pathways for neuronal entry. Genes identified as required for monomeric or fibrillar tau uptake are significantly overlapping (hypergeometric test, $p<0.001$). The 11 genes identified in both screens are shown on the right side.

(B) Subunits of protein complexes that are significantly enriched in the combined set of genes required for uptake of either form of tau. The colour indicates the positive enrichment score in the monomeric (M) and fibrillar (F) screens respectively. Only subunits identified as required in either screen are shown (orange if identified in fibrillar screens, purple if identified in monomeric screens, bold green if identified in both). FDR < 0.05 (*), <0.01 (**), < 0.001 (***).

(C) Positions of genes identified as significantly enriched in our CRISPR screens in the cellular compartments associated with the gene encoded proteins, using the COMPARTMENTS dataset (FDR < 0.05). Genes influencing uptake of monomeric (purple), fibrillar (orange) or both (green) forms of tau are ordered using the positive enrichment ranking for each cellular compartment, where appropriate genes appear in multiple compartments. See also Extended Data Fig. 3 and Supplementary Table 5.

Fig. 4. Neuronal uptake of extracellular tau shares functional similarities with endocytic pathways involved in viral entry

(A,B) Effect of endocytosis and PI3-kinase activity inhibition on neuronal uptake of extracellular monomeric (A) and fibrillar tau-pHrodo (B). Neurons were pre-incubated with either 100 μM Dynasore, 1 μM PIK93, 0.1 μM wortmannin or vehicle control (0.1% [v/v] DMSO) for one week, before addition of tau-pHrodo. pHrodo-positive objects were counted over 10 hr at 45-minute intervals. Object measurements are displayed over time and scatter plots of the final time point (dashed line) are shown; bars indicate mean. Four wells per treatment, and at least 20 fields of view per well.

(C,D) Effect of autophagy and vesicular transport inhibition on neuronal uptake of extracellular monomeric (C) and fibrillar tau-pHrodo (C) into low-pH compartments. Neurons were pre-incubated for 24 hr with either 1 μM Brefeldin, 0.1 μM Bafilomycin A or vehicle control (0.1% [v/v] DMSO) using the same experimental conditions and parameters as in (A). The number of pHrodo positive objects was measured as in (E-F; 7 wells per treatment). Significance was determined using one-way ANOVA ($*p < 0.05$, $**p < 0.01$, $***p < 0.001$, Dunnet's test for multiple comparisons).

(E) The sets of genes required for human neuronal uptake of monomeric, fibrillar or either form of tau significantly overlap with the sets of genes required for receptor-mediated endocytosis of Influenza A, Zika and SARS-CoV2 viruses, but not macropinocytosis of Ebola virus. Gene sets required for entry were defined from their respective screens using a threshold of FDR < 0.05 and hypergeometric tests were used to evaluate significance of overlap between gene sets (FDR-corrected $p^* < 0.05$, $p^{**} < 0.01$, $p^{***} < 0.001$).

(F) Diagram of cellular compartments showing genes shared between tau uptake (FDR < 0.05) and viral entry screens and their predicted roles in tau uptake and virus life cycle. Genes are marked by a shape corresponding to Influenza A virus (diamond), Zika (circle) or SARS-CoV2 virus entry (square) and coloured according to monomeric (purple), fibrillar (orange) or either form of tau (green). See also Extended Data Fig. 4 and Supplementary Table 6.

Fig. 5. LRRK2 gain and loss of function mutations affect the endolysosomal system in excitatory neurons

(A) LRRK2 heterozygous and homozygous knockout neurons do not exhibit an endosomal phenotype. Representative immunohistochemistry of neurons from isogenic control, heterozygous (+/-) and homozygous (-/-) LRRK2 knockout human iPSCs (60 days after induction), immunostained for neuronal β3-tubulin (TUJ1, green), early endosomes (EEA1, red) and nuclei were counterstained (DAPI, blue). Scale bar, 10 μm. (B) No significant changes in the average size of early endosomes (EEA positive vesicles; μm2) in heterozygous and homozygous (null) LRRK2 knockout neurons compared with isogenic control (n = >5 images).

(C) LRRK2 homozygous knockout neurons display enlarged, abnormal lysosomes. Representative immunohistochemistry of neurons from isogenic control, heterozygous (+/-) and homozygous (-/-) LRRK2 knockout human iPSCs (60 days after induction), immunostained for neuronal β3-tubulin (TUJ1, green), lysosomes (LAMP1, red) and nuclei were counterstained (DAPI, blue). Scale bar, 10 μm. (D) Significant increase in average late endosome/lysosome area (LAMP1 positive vesicles; μm2) in homozygous LRRK2 knockout neurons compared with isogenic controls (n = >5 images).

(E-H) Neurons heterozygous for the LRRK2 G2019S mutation display enlarged, abnormal endosomes and lysosomes. Representative confocal images of human iPSC neurons from isogenic control and with LRRK2 G2019S mutation (heterozygous; 60 days after induction), immunostained for neuronal β3-tubulin (TUJ1, green), (E) endosomes (EEA1, red) or (G) lysosomes (LAMP1, red) and nuclei were counterstained (DAPI, blue). Scale bar, 10 μm. Significant increase in average area of early (F) and late endosomes/lysosomes (H) (EEA1/LAMP1 positive vesicles; μm2) in LRRK2 G2019S neurons compared with isogenic controls (n = >5 images).

Fig. 6. LRRK2 gain and loss of function mutations affect uptake of extracellular tau, a-synuclein and a-beta

Neurons with LRRK2 gain and loss of function mutations differ in their ability to take up extracellular proteins involved in neurodegeneration. Isogenic control, LRRK2 heterozygous (-/+), homozygous (-/-) null or LRRK2 G2019S mutant neurons (65 days after induction) were incubated with 90 nM transferrin (Tfn) Alexa 633 nm and either monomeric wild-type (A), monomeric P301S (B) or fibrillar P301S (C) tau Dylight 488 nm for 4 hr before dissociation into single cells and analysis by flow cytometry. Neurons from each of the genotypes were also incubated with α-synuclein (D), β-amyloid (1-42) (E) HiLyte 488 nm or epidermal growth factor (EGF) Fluorescein 488 nm (F) and analysed in the same way as the tau protein derivatives. For each genotype and cell line indicated, the percentage of low protein uptake in transferrin positive neurons (indicated by the black outlined boxes) was compared to the mean (dashed line) of protein uptake of control neurons and displayed as fold change (log2). Significance was determined using one-way ANOVA ($*p < 0.05$, $**p < 0.01$, $***p < 0.001$ Dunnet's test for multiple comparisons; circles, triangles and squares represent independent experiments; n=>3). See also Extended Data Fig. 6.

Fig. 7. Inhibition of the LRRK2 kinase reduces neuronal uptake of monomeric and fibrillar tau

(A, B) Neurons treated with LRRK2 kinase activity inhibitors do not exhibit a lysosomal dysfunction phenotype. Representative confocal images of neurons (60 days after induction) treated for one week with vehicle control (0.1% [v/v] DMSO), 1μM MLi-2 or 10μM GSK3357679A (GSK-X), immunostained for neuronal β3-tubulin (TUJ1, green), lysosomes (LAMP1; red) and nuclei were counterstained (DAPI, blue). Scale bar, 10 μm. No significant changes were detected in the average lysosome area (LAMP1 positive vesicles; μm2) in neurons treated with LRRK2 kinase activity inhibitors compared with vehicle control (n = >5 images).

(C-E) Entry of monomeric and fibrillar tau into neurons is inhibited by LRRK2 kinase inhibitors (MLi-2 and GSK-X), in a concentration dependent manner. Human iPSC-derived neurons were pre-incubated with 1 μM MLi-2, 1 μM or 10 μM GSK-X or vehicle control (0.1% [v/v] DMSO) for one week, before acute addition of pHrodo-labelled monomeric tau (C), fibrillar tau (D) or transferrin (E). Live-imaging captured pHrodo-labelled protein uptake into low-pH compartments in neurons (65 days after induction) and the number of pHrodo-positive objects was measured over 7.3 hr at 45-minute intervals. Object measurements are displayed over time and scatter plots of the final time point (dashed line) are shown; bars indicate mean. At least three wells per treatment, and >20 fields of view per well. Significance was determined using one-way ANOVA ($*p < 0.05$, $**p < 0.01$, Dunnet's test for multiple comparisons). See also Extended Data Fig. 7.

Extended Data Fig. 1. Development and optimisation of CRISPR screen for tau uptake in human iPSC-derived excitatory neurons

(A) Construct of KOLF2-C1 Cas9 cell line. KOLF2-C1 parent cell line genetically engineered at the AAVS1 locus to constitutively express humanized Cas9 with N-terminal FLAG tag (three repeats) and SV40 nuclear localisation signal (NLS) and C-terminal nucleoplasmin NLS from CAG promoter (CMV/chicken β-actin promoter).

(B) Gene expression analysis of iPSC-derived neuronal progenitor cells from KOLF2-C1 (parental line) and KOLF2-C1 Cas9 (constitutively expressing Cas9), 35 days after induction. Selected genes whose expression is specific or enriched in particular regions and/or cell types are shown from a panel of 200 genes (see Experimental Procedures for details).

(C) Analysis of the proportion of MAP2 positive KOLF2-C1 Cas9 neurons 60 days after induction. Neurons were dissociated into single cells and immunostained using MAP2 antibody conjugated to PE and analysed by flow cytometry. To establish threshold levels for MAP2 positive neurons (bold horizontal bar) unstained control neurons were analysed.

(D,E) Optimising concentration of tau protein to achieve saturating levels of extracellular tau uptake during acute treatment, measured by flow cytometry. Graph reports percentage of tau-positive neurons over time after tau incubation initiation, with concentration of tau protein as indicated.

(F) Percentage of whole-genome CRISPR gRNA library lentivirus-transduced (BFP+) neurons in tau uptake FACS screens.

(G) Total number of lentivirus-transduced (BFP+) neurons collected by flow cytometry in each screen (left axis) and corresponding library coverage (n. cells/n. gRNAs) (right axis).

(H) Percentage of lentivirus-transduced neurons collected from monomeric and fibrillar tau uptake screens that are transferrin positive and tau negative.

(I) Total number of transferrin positive, tau negative lentivirus-transduced neurons collected by flow cytometry in each screen (left axis) and corresponding library coverage (n. cells/n. gRNAs) (right axis).

(J) Distribution of median normalized log2 guide RNA counts from transferrin positive and either tau positive (+) or negative (-) neurons collected from monomeric (purple; 2 screens) and fibrillar (orange; 3 screens) tau uptake screens.

(K) Percentage of CRISPR gRNA detected in transferrin positive and either tau positive (POSPOS) or negative (NEGPOS) neurons collected from tau uptake FACS screens.

Extended Data Fig. 2. Identification of genes involved in the uptake of structurally distinct forms of tau by human cortical neurons via low pH intracellular compartments

(A,B) CRISPR gRNA log fold change (LFC) between transferrin positive and either tau positive (+) or negative (-) neurons collected from monomeric (A) and fibrillar (B) tau uptake screens analysed using the MAGeCK algorithm. Guides for the five highest ranked genes (gene names indicated) are highlighted on guide density plots.

Genes required for uptake of monomeric (C), fibrillar (D) tau code for proteins with a significantly higher than random localisation score in particular cellular compartments in the COMPARTMENTS dataset (FDR < 0.05). Significantly enriched compartments are coloured based on the strength of enrichment (log2 fold-change) whereas non-significant compartments are left white.

(E) Time-lapse (0- to 4-hr) images showing uptake into iPSC-derived human neurons (60 days after induction) of extracellular monomeric tau conjugated to a pH-sensitive dye (inverse relationship between fluorescence and pH). Neurons and tau protein were individually pre-incubated with either 10nM RAP chaperone, 100nM LRP1 domain IV peptide or vehicle control (PBS) for 3 hrs prior to combining the tau incubations with neurons and live imaging of neuronal uptake of tau. Bright-field (grey scale in merge) and pH-sensitive fluorescent signal (pHrodo; red in merge) were captured using automated imaging on the Opera Phenix platform (PerkinElmer). Scale bar, 100 μm.

(F) None of the forms of tau were acutely toxic to neurons over a 16 hr period, as measured by extracellular LDH activity (3 wells per treatment), in the presence of 25nM Monomeric tau, 150nM (monomer molar equivalent) fibrillar or postmortem tau.

(G) Extracellular LDH activity was also used to determine neuronal viability in the presence of vehicle (PBS), 10nM RAP chaperone or 100nM LRP1 domain IV peptide (after treatment for one week; 3 wells per treatment). Error bars indicate SD. Significance was determined using one-way ANOVA ($*p < 0.05$, $**p < 0.01$, Dunnet's test for multiple comparisons).

Extended Data Fig. 3. Comparison of genes required for monomeric and fibrillar tau entry by human cortical neurons

(A) Heat map showing a representative selection of significantly enriched terms annotating the 431 genes significantly enriched for either monomeric or fibrillar tau uptake. The black colour scale indicates the significance level (-log10 FDR). Rows are sorted in order of significance, also see Supplementary Table 3. The central heatmap shows which of the enriched genes is annotated with each term.

(B) PSICQUIC-derived network of experimentally validated physical interactions between proteins encoded by genes identified in either screen. Nodes are colour-coded depending on whether the corresponding gene was identified as required for monomeric (purple) or fibrillar (orange) tau uptake, or both (green). Some notable complexes are highlighted with circles. Interactions disconnected from the main network are not shown.

(C) The direct interactors of LRRK2, the most connected node, are highlighted in the protein interaction network, indirect interactions and genes unconnected to LRRK2 appear in grey.

(D) Genes required for uptake of either monomeric or fibrillar tau code for proteins with a significantly higher than random localisation score in particular cellular compartments in the COMPARTMENTS dataset (FDR < 0.05). Significantly enriched compartments are coloured based on the strength of enrichment (log2 fold-change) whereas non-significant compartments are left white.

Extended Data Fig. 4. Cellular mechanisms for tau uptake and processing by human excitatory neurons in relation to endocytosis and viral entry CRISPR screens

(A) Extracellular LDH activity was used to determine neuronal viability in the presence of vehicle (0.1% [v/v] DMSO), 100μM Dynasore, 1μM PIK93 or 0.1 μM Wortmannin (after treatment for one week) (B), and for 1μM Brefeldin or 0.1μM Bafilomycin A (after treatment for 24hr) (I). Only Bafilomycin A had a modest effect of neuronal viability (3 wells per treatment). Error bars indicate SD. Significance was determined using one-way ANOVA ($*p < 0.05$, $**p < 0.01$, Dunnet's test for multiple comparisons).

(C) Neuronal uptake of tau protein requires cargo-specific endocytic adapters. Comparison of sets of genes required for tau uptake with genes identified in screens for endocytosis of either transferrin or epidermal growth factor (EGF), shows significant overlap between monomeric tau uptake and transferrin endocytosis, but no other significant overlaps between the gene sets.

(D) Genes involved in tau uptake do not significantly overlap with sets of genes identified as phagocytosis regulators in screens performed with distinct substrates, varying in their diameter (μm) and charge.

(E) Heatmap showing functional annotations enriched among genes required for the uptake of either form of tau and Influenza A, Zika or SARS-CoV2 virus entry (representative term selection).

(F) Genes required for either monomeric or fibrillar tau uptake and Influenza A, Zika or SARS-CoV-2 viral entry code for proteins with a significantly higher than random localisation score in particular cellular compartments in the COMPARTMENTS dataset (FDR < 0.05). Significantly enriched compartments are coloured based on the strength of enrichment (log2 fold-change) whereas non-significant compartments are left white.

Extended Data Fig. 5. Neuronal gene expression and LRRK2 protein levels in iPSC-derived cortical neurons with LRRK2 gain and loss of function mutations

(A,B) Gene expression (Nanostring) analysis of iPSC-derived neuronal progenitor cells from KOLF2-C1 (parental line; Isogenic control), LRRK2 heterozygous null (LRRK2 -/+), LRRK2 homozygous null (LRRK2 -/-) and LRRK2 heterozygous G2019S, 35 (A) and between 64-76 (B) days after induction. Selected genes whose expression is specific or enriched in particular regions and/or cell types are shown from a panel of 200 genes (see Experimental Procedures for details), demonstrating that the inductions generated primarily cortical progenitor cells, with some ventral interneuron progenitor cells, which subsequently generate excitatory and inhibitory neurons.

(C) LRRK2 protein levels in iPSC from KOLF2-C1 (parental line; Isogenic control), LRRK2 heterozygous null (LRRK2 +/-), LRRK2 homozygous null (LRRK2 -/-) and LRRK2 heterozygous G2019S, measured by AlphaLISA assay (see Methods for details). LRRK2 +/- cells have reduced LRRK2 protein relative to the parental cell, whereas LRRK2 -/- cells have protein around the detection threshold of the assay.

Extended Data Fig. 6. Uptake of transferrin and dextran by LRRK2 gain and loss of function mutation-expressing neurons

(A) Flow cytometry gating strategy for detection of transferrin and indicated cargo protein uptake into iPSC-derived isogenic control neurons (65 days after induction). Left panels show discrimination based on scatter parameters of neurons incubated with either no treatment (red) or extracellular transferrin (green), monomeric tau (orange) or fibrillar tau (blue). Black polygons and bold horizontal bars indicate gates applied to isolate population of single neurons that endocytose transferrin. To establish threshold levels for positive protein uptake (bold horizontal bars) neurons without transferrin (red) or tau (green contours) incubation were analysed.

(B) Fluorescent intensity of either monomeric or fibrillar Dylight 488nm low tau protein uptake populations are indicated by black polygons.

(C) Isogenic control, LRRK2 heterozygous (+/-), homozygous (-/-) null or LRRK2 G2019S mutant neurons (65 days after induction) were incubated with 90 nM transferrin (Tfn) Alexa 633 nm or Dextran Fluorescein 488 nm (D) for 4 hr before dissociation into single cells and analysis by flow cytometry. For each genotype and cell line indicated, the percentage of cells with low protein uptake (indicated by the black outlined polygons) was compared to the mean (dashed line) of protein uptake of control neurons and displayed as fold change (log2). Significance was determined using one-way ANOVA ($*p < 0.05$, $**p < 0.01$, Dunnett's test for multiple comparisons; circles and triangles represent independent experiments; n=>3).

(E-G) Biological replicate flow cytometry assays of the effect of LRRK2 G2019S mutation on neuronal uptake of extracellular tau. Isogenic control and LRRK2 G2019S mutant neurons (65 days after induction) were incubated with 90 nM transferrin (Tfn) Alexa 633 nm and either monomeric wild-type (E), or fibrillar P301S (F) tau Dylight 488 nm, or transferrin alone (G), for 4 hr before dissociation into single cells and analysis by flow cytometry (ThermoFisher Attune CytPix). For LRRK2 G2019S mutant neurons, the percentage of cells with low protein uptake (in neurons gated for transferrin uptake) was compared to the mean (dashed line) of protein uptake of control neurons and displayed as fold change (log2). Significance was determined using unpaired t-test ($***p < 0.001$; n=4 for controls and n=12 for LRRK2 G2019S; neurons generated from 2 and 4 independent neural inductions from control and LRRK2 G2019S iPSCs, respectively).

(H) LRRK2 homozygous null neurons have increased levels of tau receptor protein LRP1 at the neuronal surface compared with isogenic controls. LRRK2 heterozygous and homozygous null neurons (60 days after induction) were surface biotinylated and Neutravidin-coated particles used to capture biotinylated membrane proteins. Surface abundance of indicated proteins were measured by immunoblotting. (I) Cell surface levels of

LRP1 normalised to N-cadherin are shown for each genotype. Significance was determined using one-way ANOVA ($*p < 0.05$, $**p < 0.01$, Dunnet's test for multiple comparisons, n=3).

Extended Data Fig. 7. Effect of LRRK2 kinase activity inhibitors on the endolysosomal system of human cortical neurons

(A-B) Neurons treated with LRRK2 kinase activity inhibitors do not exhibit an endosomal or lysosomal phenotype. (A) Representative immunohistochemistry of neurons (60 days after induction) treated for one week with vehicle control (0.1% [v/v] DMSO), 1μM MLi-2 or 10μM GSK-X, immunostained for neuronal β3-tubulin (TUJ1, green), early endosomes (EEA1; red) and nuclei were counterstained (DAPI, blue). Scale bar, 10 μm. (B) No significant changes in the average size of early endosomes (EEA positive vesicles; μm2) in neurons compared with isogenic control (n = >5 images).

(C) Extracellular LDH activity was used to assess neuronal viability in the presence of vehicles (0.1% [v/v] DMSO), 1μM MLi-2, 1μM or 10μM GSK-X (GSK3357679A; treatment for one week). Only 1μM MLi-2 had a modest effect of neuronal viability (3 wells per treatment). Error bars indicate SD. Significance was determined using one-way ANOVA ($*p < 0.05$, Dunnet's test for multiple comparisons).

(D) Effect of inhibition of LRRK2 kinase activity on neuronal surface levels of tau receptor protein LRP1. Neurons were pre-incubated with either 1 μM MLi-2, 10 μM GSK-X or vehicle control (0.1% [v/v] DMSO) for one week prior to cell surface biotinylation (61 days after induction) followed by capture of biotinylated membrane proteins using Neutravidin-coated particles. Surface abundance of indicated proteins were examined by immunoblotting. (E) Cell surface levels of LRP1 normalised to N-cadherin are shown for each of the treatments.

Supplementary Table 1. Summary of CRISPR screens for tau uptake

Summary of the CRISPR screens reported here for tau uptake, including numbers of cells analysed and proportion of neurons exhibiting reduced tau uptake as a proportion of gRNA expressing cells. Figures in brackets are the percentages of the total events.

Supplementary Table 2. Summary of gene-level results for monomeric and fibrillar tau screens

Summary of MAGeCK results from CRISPR screens for tau uptake, including positive enrichment and log-fold change. Where the names of target genes in the library have been updated, the most recent gene names, which were used for pathway enrichment analysis, are indicated for significant hits (pval <0.01) in the last column.

Supplementary Table 3. Pathway enrichment analysis of hits of tau uptake screens

gProfiler2 output showing significantly enriched pathways in the sets of significant hits (pval <0.01) found in the CRISPR screens for monomeric tau, fibrillar tau, or either.

Supplementary Table 4. Summary CRISPR Guide sequences targeting individual genes and statistical analysis for validation

Genes selected from tau uptake screen for monomeric tau uptake validation, their positive MAGeCK ranking in both monomeric and fibrillar tau uptake screens, Dunnett's multiple comparisons test, summary of statistical comparison and adjusted p values.

Supplementary Table 5. Analysis of COMPARTMENTS localisation score enrichment for hits of tau uptake screens

Normalised localisation score for selected terms in the COMPARTMENTS database for the sets of significant hits (pval <0.01) found in the CRISPR screens for monomeric tau, fibrillar tau, or either. The mean for the corresponding simulated gene sets, log-fold enrichment and bootstrapped p-value are also indicated.

Supplementary Table 6. Summary of viral overlaps and related pathway and localisation enrichment analysis

Summary of overlaps between tau uptake screens and other published screens for viral uptake, phagocytosis, or endocytosis. The results of pathway and COMPARTMENT localisation enrichment analysis is provided for the set of overlapping genes between either the monomeric or fibrillar tau screens and either of the Zika, Influenza A, or Coronavirus screens.

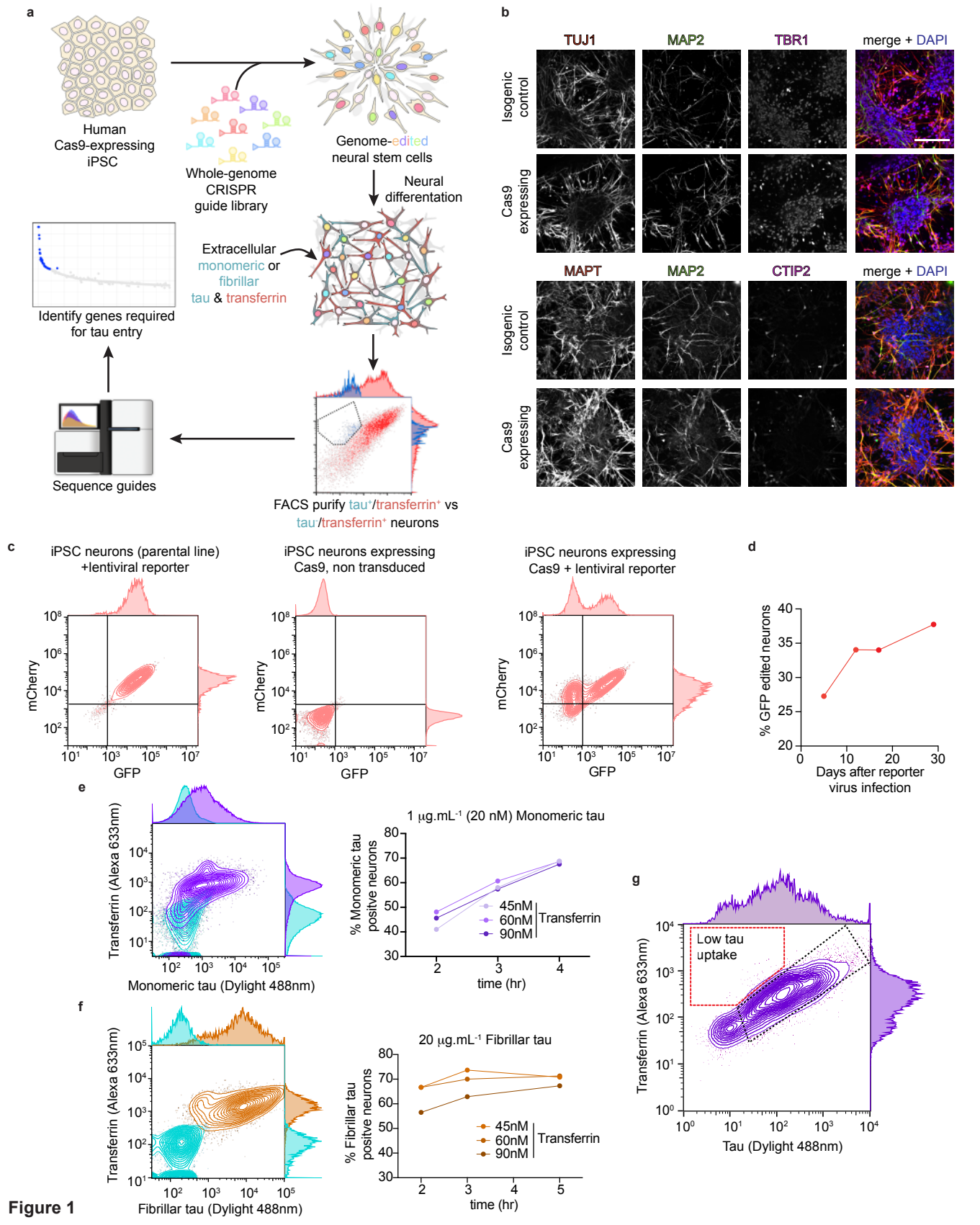
a
Human Cas9-expressing iPSC
Whole-genome CRISPR guide library
Genome-edited neural stem cells
Neural differentation
Extracellular monomeric or fibrillar tau & transferrin
FACS purify tau+/transferrin+ vs tau-/transferrin+ neurons
Sequence guides
Identify genes required for tau entry
b
TUJ1
MAP2
TBR1
merge + DAPI
Isogenic control
Cas9 expressing
MAPT
MAP2
CTIP2
merge + DAPI
Isogenic control
Cas9 expressing
c
iPSC neurons (parental line) +lentiviral reporter
iPSC neurons expressing Cas9, non transduced
iPSC neurons expressing Cas9 + lentiviral reporter
mCherry
GFP
d
% GFP edited neurons
Days after reporter virus infection
e
Transferrin (Alexa 633nm)
Monomeric tau (Dylight 488nm)
1 µg.mL-1 (20 nM) Monomeric tau
% Monomeric tau positve neurons
45nM
60nM
90nM
Transferrin
time (hr)
f
Transferrin (Alexa 633nm)
Fibrillar tau (Dylight 488nm)
20 µg.mL-1 Fibrillar tau
% Fibrillar tau positve neurons
45nM
60nM
90nM
Transferrin
time (hr)
g
Low tau uptake
Transferrin (Alexa 633nm)
Tau (Dylight 488nm)

Figure 1

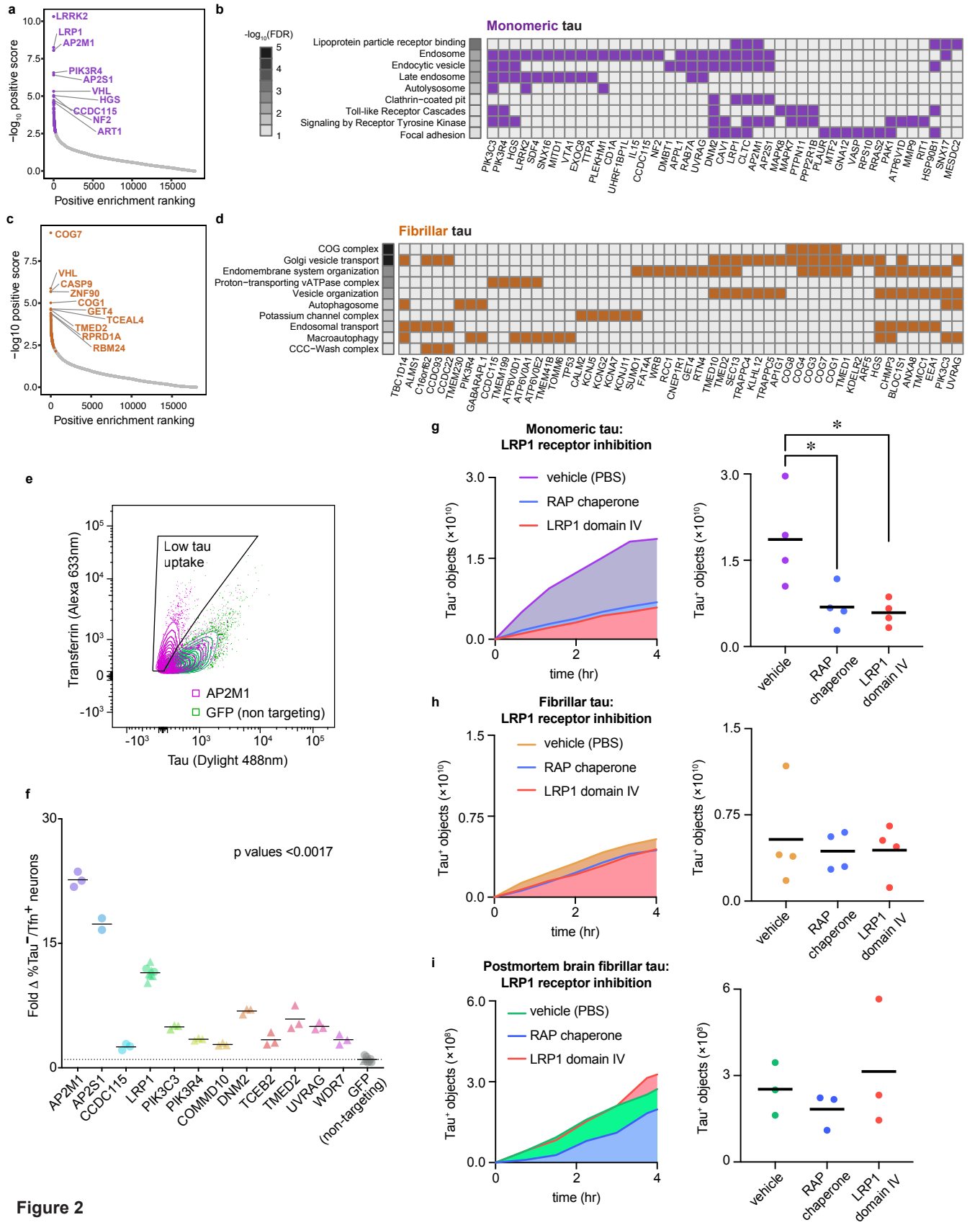
a
LRRK2
LRP1
AP2M1
PIK3R4
AP2S1
VHL
HGS
CCDC115
NF2
ART1
−log10 positive score
Positive enrichment ranking
b
Monomeric tau
-log10(FDR)
Lipoprotein particle receptor binding
Endosome
Endocytic vesicle
Late endosome
Autolysosome
Clathrin−coated pit
Toll-like Receptor Cascades
Signaling by Receptor Tyrosine Kinase
Focal adhesion
c
COG7
VHL
CASP9
ZNF90
COG1
GET4
TCEAL4
TMED2
RPRD1A
RBM24
−log10 positive score
Positive enrichment ranking
d
Fibrillar tau
COG complex
Golgi vesicle transport
Endomembrane system organization
Proton−transporting vATPase complex
Vesicle organization
Autophagosome
Potassium channel complex
Endosomal transport
Macroautophagy
CCC−Wash complex
e
Low tau uptake
Transferrin (Alexa 633nm)
Tau (Dylight 488nm)
AP2M1
GFP (non targeting)
f
p values <0.0017
Fold Δ %Tau⁻/Tfn⁺ neurons
AP2M1
AP2S1
CCDC115
LRP1
PIK3C3
PIK3R4
COMMD10
DNM2
TCEB2
TMED2
UVRAG
WDR7
GFP (non-targeting)
g
Monomeric tau: LRP1 receptor inhibition
vehicle (PBS)
RAP chaperone
LRP1 domain IV
Tau⁺ objects (×10¹⁰)
time (hr)
vehicle
RAP chaperone
LRP1 domain IV
h
Fibrillar tau: LRP1 receptor inhibition
vehicle (PBS)
RAP chaperone
LRP1 domain IV
Tau⁺ objects (×10¹⁰)
time (hr)
vehicle
RAP chaperone
LRP1 domain IV
i
Postmortem brain fibrillar tau: LRP1 receptor inhibition
vehicle (PBS)
RAP chaperone
LRP1 domain IV
Tau⁺ objects (×10⁸)
time (hr)
vehicle
RAP chaperone
LRP1 domain IV

Figure 2

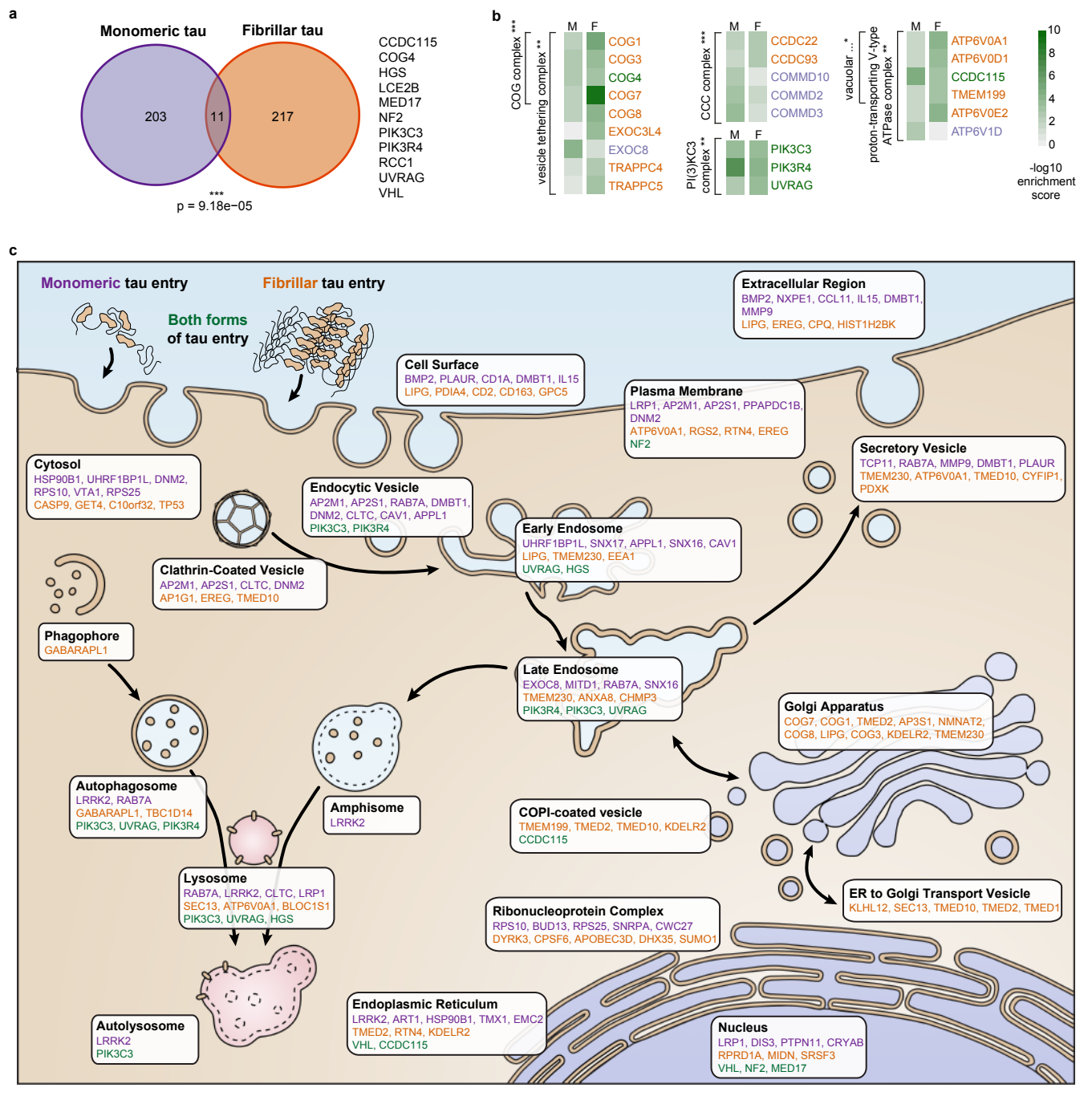
a
Monomeric tau
Fibrillar tau
203
11
217
***
p = 9.18e−05
CCDC115
COG4
HGS
LCE2B
MED17
NF2
PIK3C3
PIK3R4
RCC1
UVRAG
VHL
b
M F
COG complex ***
vesicle tethering complex **
COG1
COG3
COG4
COG7
COG8
EXOC3L4
EXOC8
TRAPPC4
TRAPPC5
CCC complex ***
CCDC22
CCDC93
COMMD10
COMMD2
COMMD3
PI(3)KC3 complex **
PIK3C3
PIK3R4
UVRAG
vacuolar ... *
proton-transporting V-type ATPase complex **
ATP6V0A1
ATP6V0D1
CCDC115
TMEM199
ATP6V0E2
ATP6V1D
10
8
6
4
2
0
-log10 enrichment score
c
Monomeric tau entry
Fibrillar tau entry
Both forms of tau entry
Extracellular Region
BMP2, NXPE1, CCL11, IL15, DMBT1, MMP9
LIPG, EREG, CPQ, HIST1H2BK
Cell Surface
BMP2, PLAUR, CD1A, DMBT1, IL15
LIPG, PDIA4, CD2, CD163, GPC5
Plasma Membrane
LRP1, AP2M1, AP2S1, PPAPDC1B, DNM2
ATP6V0A1, RGS2, RTN4, EREG
NF2
Secretory Vesicle
TCP11, RAB7A, MMP9, DMBT1, PLAUR
TMEM230, ATP6V0A1, TMED10, CYFIP1, PDXK
Cytosol
HSP90B1, UHRF1BP1L, DNM2, RPS10, VTA1, RPS25
CASP9, GET4, C10orf32, TP53
Endocytic Vesicle
AP2M1, AP2S1, RAB7A, DMBT1, DNM2, CLTC, CAV1, APPL1
PIK3C3, PIK3R4
Early Endosome
UHRF1BP1L, SNX17, APPL1, SNX16, CAV1
LIPG, TMEM230, EEA1
UVRAG, HGS
Clathrin-Coated Vesicle
AP2M1, AP2S1, CLTC, DNM2
AP1G1, EREG, TMED10
Phagophore
GABARAPL1
Late Endosome
EXOC8, MITD1, RAB7A, SNX16
TMEM230, ANXA8, CHMP3
PIK3R4, PIK3C3, UVRAG
Golgi Apparatus
COG7, COG1, TMED2, AP3S1, NMNAT2, COG8, LIPG, COG3, KDELR2, TMEM230
Autophagosome
LRRK2, RAB7A
GABARAPL1, TBC1D14
PIK3C3, UVRAG, PIK3R4
Amphisome
LRRK2
COPI-coated vesicle
TMEM199, TMED2, TMED10, KDELR2
CCDC115
Lysosome
RAB7A, LRRK2, CLTC, LRP1
SEC13, ATP6V0A1, BLOC1S1
PIK3C3, UVRAG, HGS
ER to Golgi Transport Vesicle
KLHL12, SEC13, TMED10, TMED2, TMED1
Ribonucleoprotein Complex
RPS10, BUD13, RPS25, SNRPA, CWC27
DYRK3, CPSF6, APOBEC3D, DHX35, SUMO1
Autolysosome
LRRK2
PIK3C3
Endoplasmic Reticulum
LRRK2, ART1, HSP90B1, TMX1, EMC2
TMED2, RTN4, KDELR2
VHL, CCDC115
Nucleus
LRP1, DIS3, PTPN11, CRYAB
RPRD1A, MIDN, SRSF3
VHL, NF2, MED17

Figure 3

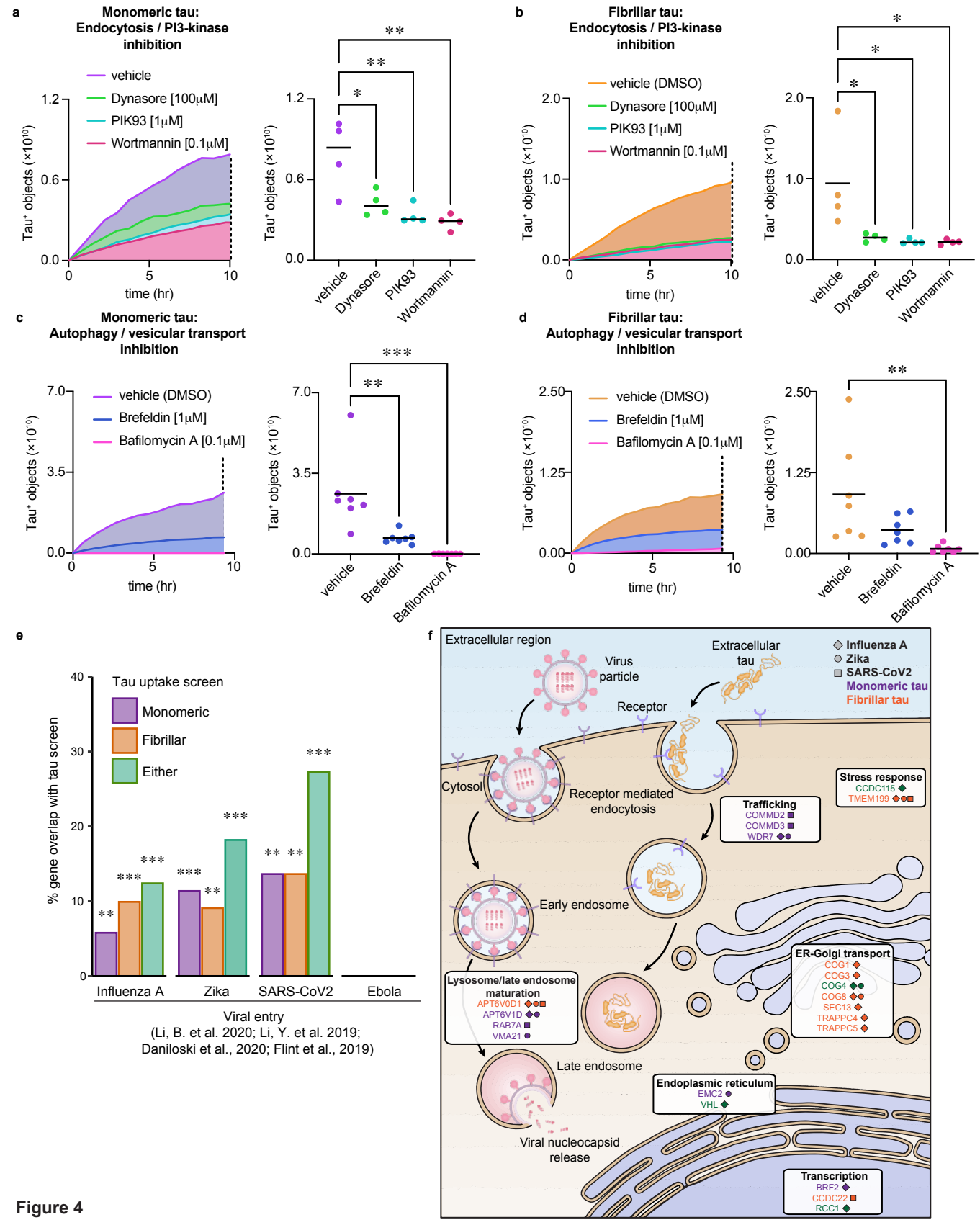
a
Monomeric tau:
Endocytosis / PI3-kinase inhibition
vehicle
Dynasore [100μM]
PIK93 [1μM]
Wortmannin [0.1μM]
Tau+ objects (×10^10)
time (hr)
vehicle
Dynasore
PIK93
Wortmannin
b
Fibrillar tau:
Endocytosis / PI3-kinase inhibition
vehicle (DMSO)
Dynasore [100μM]
PIK93 [1μM]
Wortmannin [0.1μM]
c
Monomeric tau:
Autophagy / vesicular transport inhibition
vehicle (DMSO)
Brefeldin [1μM]
Bafilomycin A [0.1μM]
Brefeldin
Bafilomycin A
d
Fibrillar tau:
Autophagy / vesicular transport inhibition
e
Tau uptake screen
Monomeric
Fibrillar
Either
% gene overlap with tau screen
Influenza A
Zika
SARS-CoV2
Ebola
Viral entry
(Li, B. et al. 2020; Li, Y. et al. 2019;
Daniloski et al., 2020; Flint et al., 2019)
f
Extracellular region
Virus particle
Extracellular tau
Receptor
Influenza A
Zika
SARS-CoV2
Monomeric tau
Fibrillar tau
Cytosol
Receptor mediated endocytosis
Stress response
CCDC115
TMEM199
Trafficking
COMMD2
COMMD3
WDR7
Early endosome
ER-Golgi transport
COG1
COG3
COG4
COG8
SEC13
TRAPPC4
TRAPPC5
Lysosome/late endosome maturation
APT6V0D1
APT6V1D
RAB7A
VMA21
Late endosome
Endoplasmic reticulum
EMC2
VHL
Viral nucleocapsid release
Transcription
BRF2
CCDC22
RCC1

Figure 4

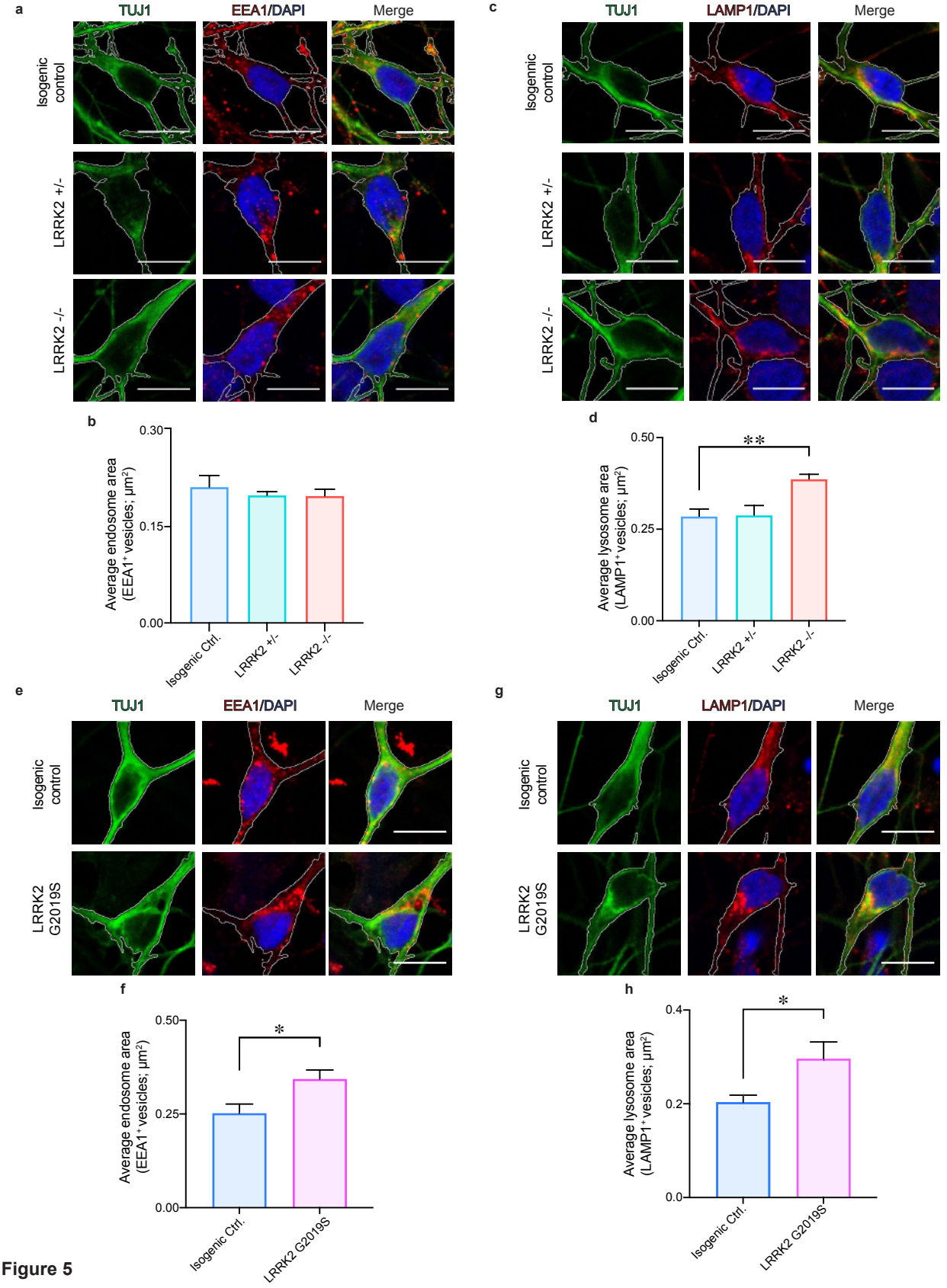
a
TUJ1
EEA1/DAPI
Merge
Isogenic control
LRRK2 +/-
LRRK2 -/-
b
Average endosome area (EEA1+ vesicles; µm²)
0.30
0.15
0.00
Isogenic Ctrl.
LRRK2 +/-
LRRK2 -/-
c
TUJ1
LAMP1/DAPI
Merge
Isogennic control
LRRK2 +/-
LRRK2 -/-
d
Average lysosome area (LAMP1+ vesicles; µm²)
0.50
0.25
0.00
**
Isogenic Ctrl.
LRRK2 +/-
LRRK2 -/-
e
TUJ1
EEA1/DAPI
Merge
Isogenic control
LRRK2 G2019S
f
Average endosome area (EEA1+ vesicles; µm²)
0.50
0.25
0.00
*
Isogenic Ctrl.
LRRK2 G2019S
g
TUJ1
LAMP1/DAPI
Merge
Isogenic control
LRRK2 G2019S
h
Average lysosome area (LAMP1+ vesicles; µm²)
0.4
0.2
0.0
*
Isogenic Ctrl.
LRRK2 G2019S

Figure 5

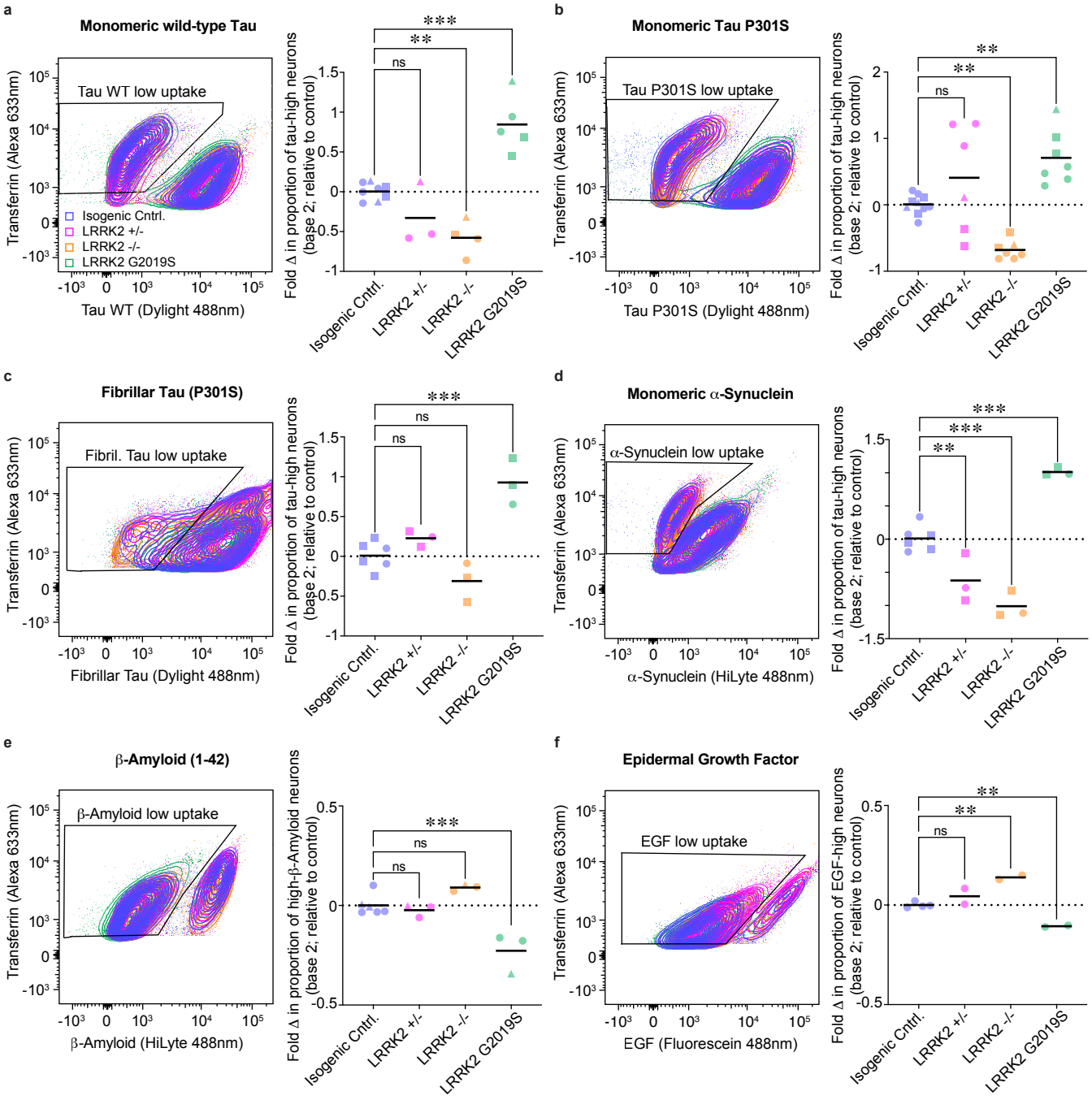
a
Monomeric wild-type Tau
Tau WT low uptake
Transferrin (Alexa 633nm)
Tau WT (Dylight 488nm)
Isogenic Cntrl.
LRRK2 +/-
LRRK2 -/-
LRRK2 G2019S
Fold Δ in proportion of tau-high neurons (base 2; relative to control)
***
**
ns
b
Monomeric Tau P301S
Tau P301S low uptake
Tau P301S (Dylight 488nm)
c
Fibrillar Tau (P301S)
Fibril. Tau low uptake
Fibrillar Tau (Dylight 488nm)
d
Monomeric α-Synuclein
α-Synuclein low uptake
α-Synuclein (HiLyte 488nm)
e
β-Amyloid (1-42)
β-Amyloid low uptake
β-Amyloid (HiLyte 488nm)
Fold Δ in proportion of high-β-Amyloid neurons (base 2; relative to control)
f
Epidermal Growth Factor
EGF low uptake
EGF (Fluorescein 488nm)
Fold Δ in proportion of EGF-high neurons (base 2; relative to control)

Figure 6

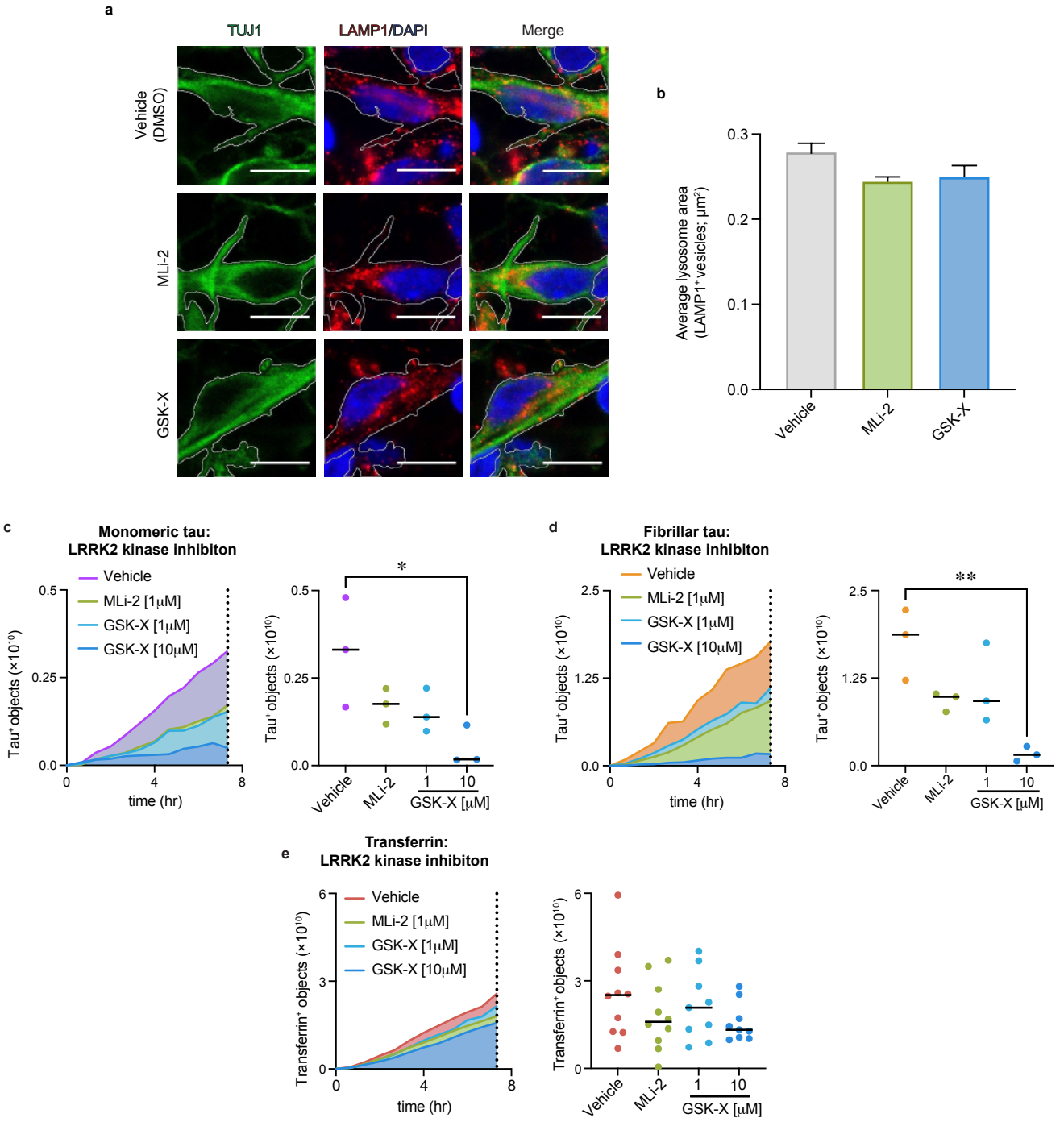
a
TUJ1
LAMP1/DAPI
Merge
Vehicle (DMSO)
MLi-2
GSK-X
b
Average lysosome area (LAMP1+ vesicles; μm²)
0.3
0.2
0.1
0.0
Vehicle
MLi-2
GSK-X
c
Monomeric tau: LRRK2 kinase inhibiton
Vehicle
MLi-2 [1μM]
GSK-X [1μM]
GSK-X [10μM]
Tau+ objects (×10¹⁰)
0.5
0.25
0.0
0
4
8
time (hr)
*
1
10
GSK-X [μM]
d
Fibrillar tau: LRRK2 kinase inhibiton
2.5
1.25
**
e
Transferrin: LRRK2 kinase inhibiton
Transferrin+ objects (×10¹⁰)
6
3

Figure 7

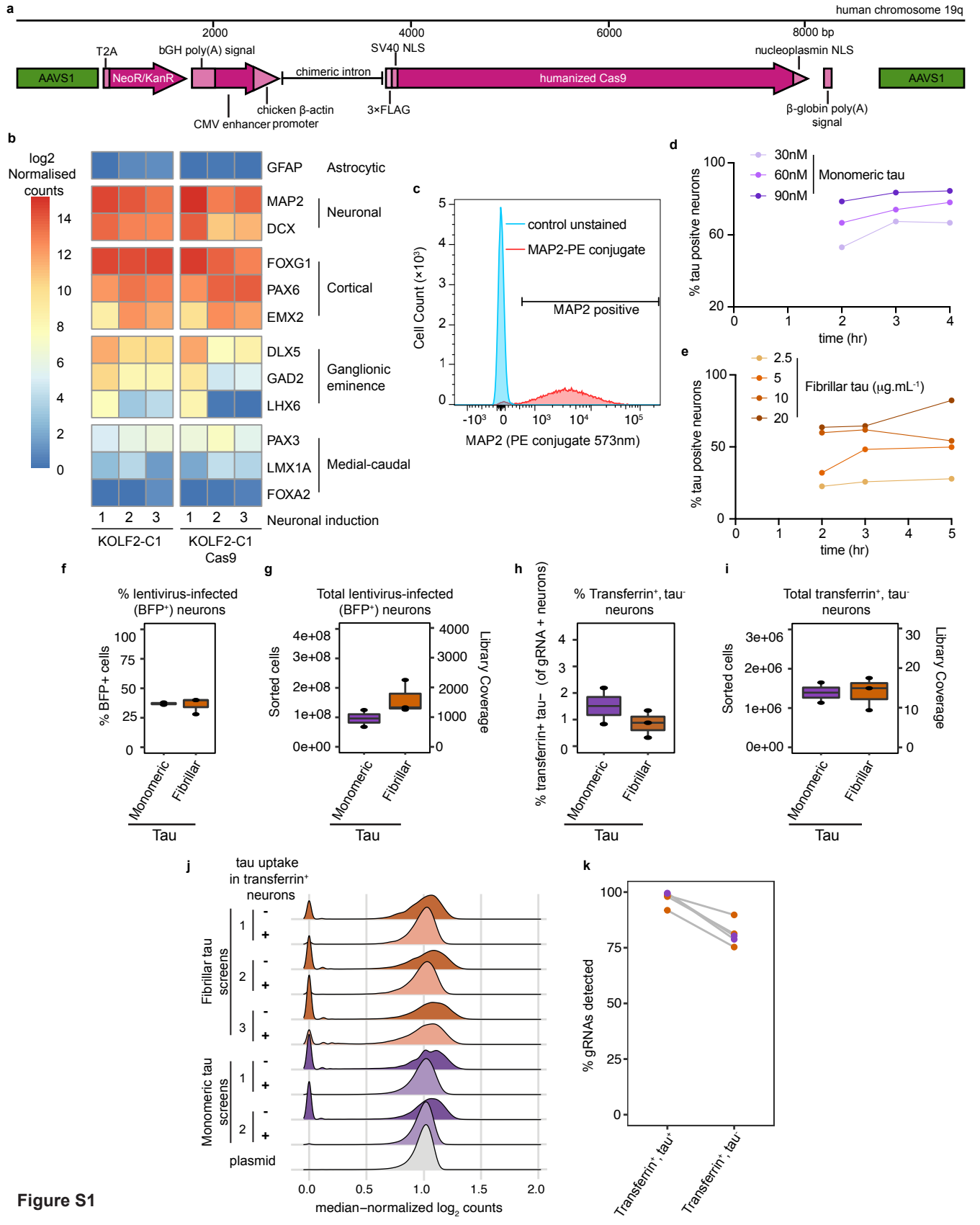
a
human chromosome 19q
2000
4000
6000
8000 bp
T2A
bGH poly(A) signal
SV40 NLS
nucleoplasmin NLS
AAVS1
NeoR/KanR
chimeric intron
humanized Cas9
AAVS1
chicken β-actin
CMV enhancer promoter
3×FLAG
β-globin poly(A)
signal
b
log2
Normalised
counts
14
12
10
8
6
4
2
0
GFAP
Astrocytic
MAP2
DCX
Neuronal
FOXG1
PAX6
EMX2
Cortical
DLX5
GAD2
LHX6
Ganglionic
eminence
PAX3
LMX1A
FOXA2
Medial-caudal
1 2 3
1 2 3
Neuronal induction
KOLF2-C1
KOLF2-C1
Cas9
c
Cell Count (×10³)
control unstained
MAP2-PE conjugate
MAP2 positive
MAP2 (PE conjugate 573nm)
d
% tau positive neurons
30nM
60nM
90nM
Monomeric tau
time (hr)
e
% tau positive neurons
2.5
5
10
20
Fibrillar tau (μg.mL⁻¹)
time (hr)
f
% lentivirus-infected
(BFP⁺) neurons
% BFP+ cells
Monomeric
Fibrillar
Tau
g
Total lentivirus-infected
(BFP⁺) neurons
Sorted cells
Library Coverage
Monomeric
Fibrillar
Tau
h
% Transferrin⁺, tau⁻
neurons
% transferrin+ tau− (of gRNA + neurons)
Monomeric
Fibrillar
Tau
i
Total transferrin⁺, tau⁻
neurons
Sorted cells
Library Coverage
Monomeric
Fibrillar
Tau
j
tau uptake
in transferrin⁺
neurons
Fibrillar tau
screens
Monomeric tau
screens
plasmid
median−normalized log₂ counts
k
% gRNAs detected
Transferrin⁺, tau⁺
Transferrin⁺, tau⁻

Figure S1

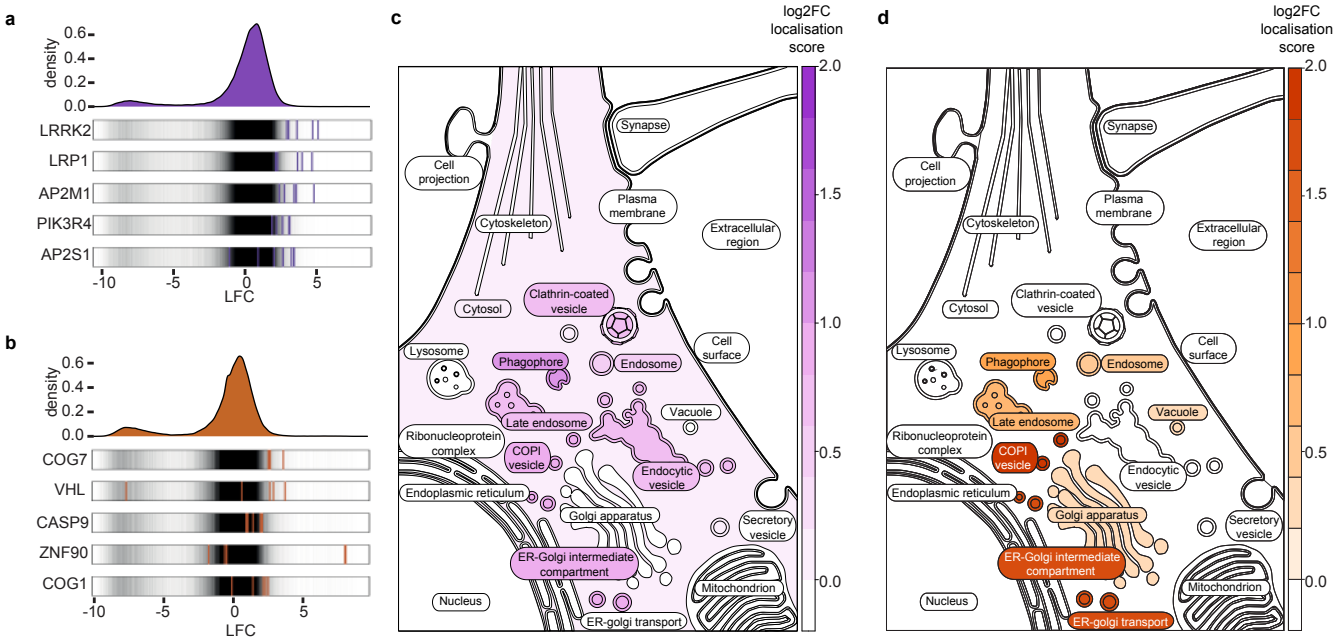
a
density
0.6
0.4
0.2
0.0
LRRK2
LRP1
AP2M1
PIK3R4
AP2S1
-10
-5
0
5
LFC
b
density
0.6
0.4
0.2
0.0
COG7
VHL
CASP9
ZNF90
COG1
-10
-5
0
5
LFC
c
log2FC
localisation
score
2.0
1.5
1.0
0.5
0.0
Synapse
Cell projection
Plasma membrane
Cytoskeleton
Extracellular region
Clathrin-coated vesicle
Cytosol
Cell surface
Lysosome
Phagophore
Endosome
Late endosome
Vacuole
Ribonucleoprotein complex
COPI vesicle
Endocytic vesicle
Endoplasmic reticulum
Golgi apparatus
Secretory vesicle
ER-Golgi intermediate compartment
Mitochondrion
Nucleus
ER-golgi transport
d
log2FC
localisation
score
2.0
1.5
1.0
0.5
0.0
Synapse
Cell projection
Plasma membrane
Cytoskeleton
Extracellular region
Clathrin-coated vesicle
Cytosol
Cell surface
Lysosome
Phagophore
Endosome
Late endosome
Vacuole
Ribonucleoprotein complex
COPI vesicle
Endocytic vesicle
Endoplasmic reticulum
Golgi apparatus
Secretory vesicle
ER-Golgi intermediate compartment
Mitochondrion
Nucleus
ER-golgi transport

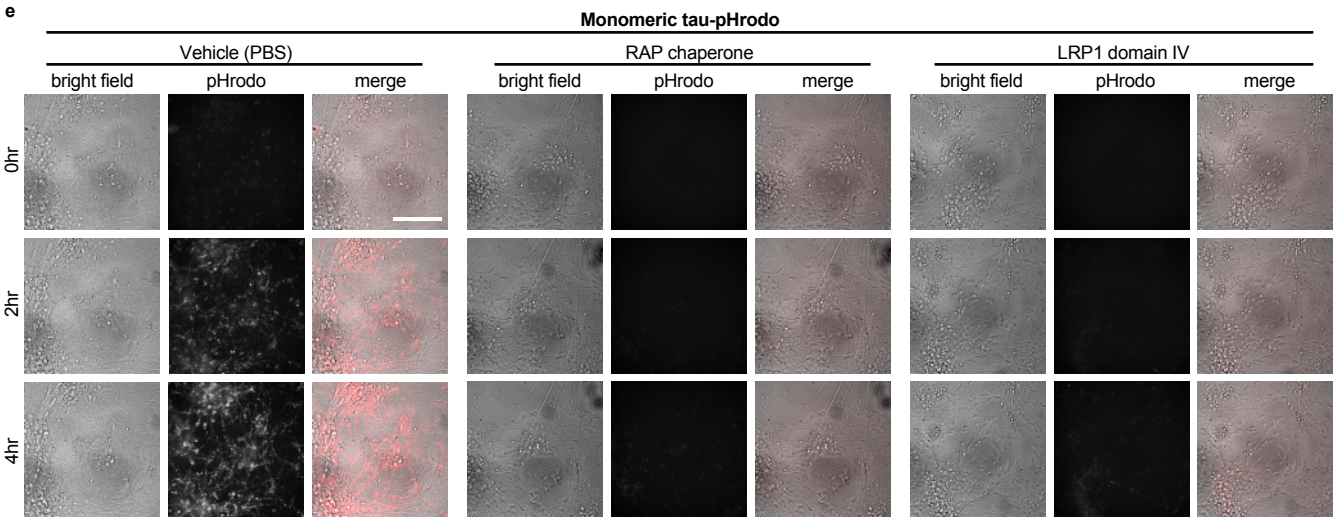
e
Monomeric tau-pHrodo
Vehicle (PBS)
RAP chaperone
LRP1 domain IV
bright field
pHrodo
merge
0hr
2hr
4hr

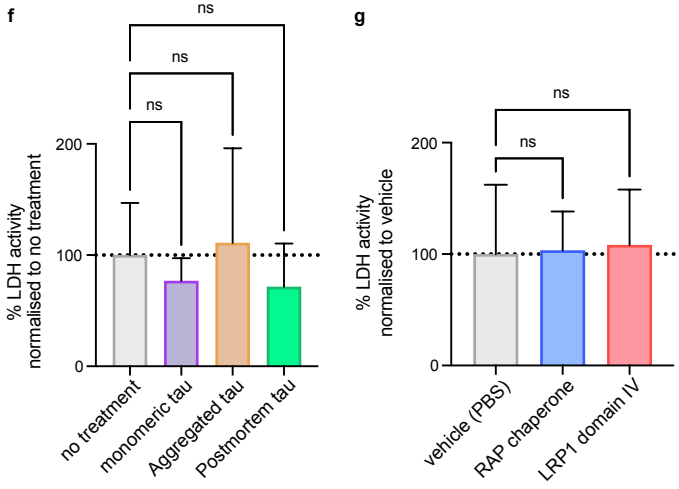
f
ns
ns
ns
% LDH activity
normalised to no treatment
200
100
0
no treatment
monomeric tau
Aggregated tau
Postmortem tau
g
ns
ns
% LDH activity
normalised to vehicle
200
100
0
vehicle (PBS)
RAP chaperone
LRP1 domain IV

Figure S2

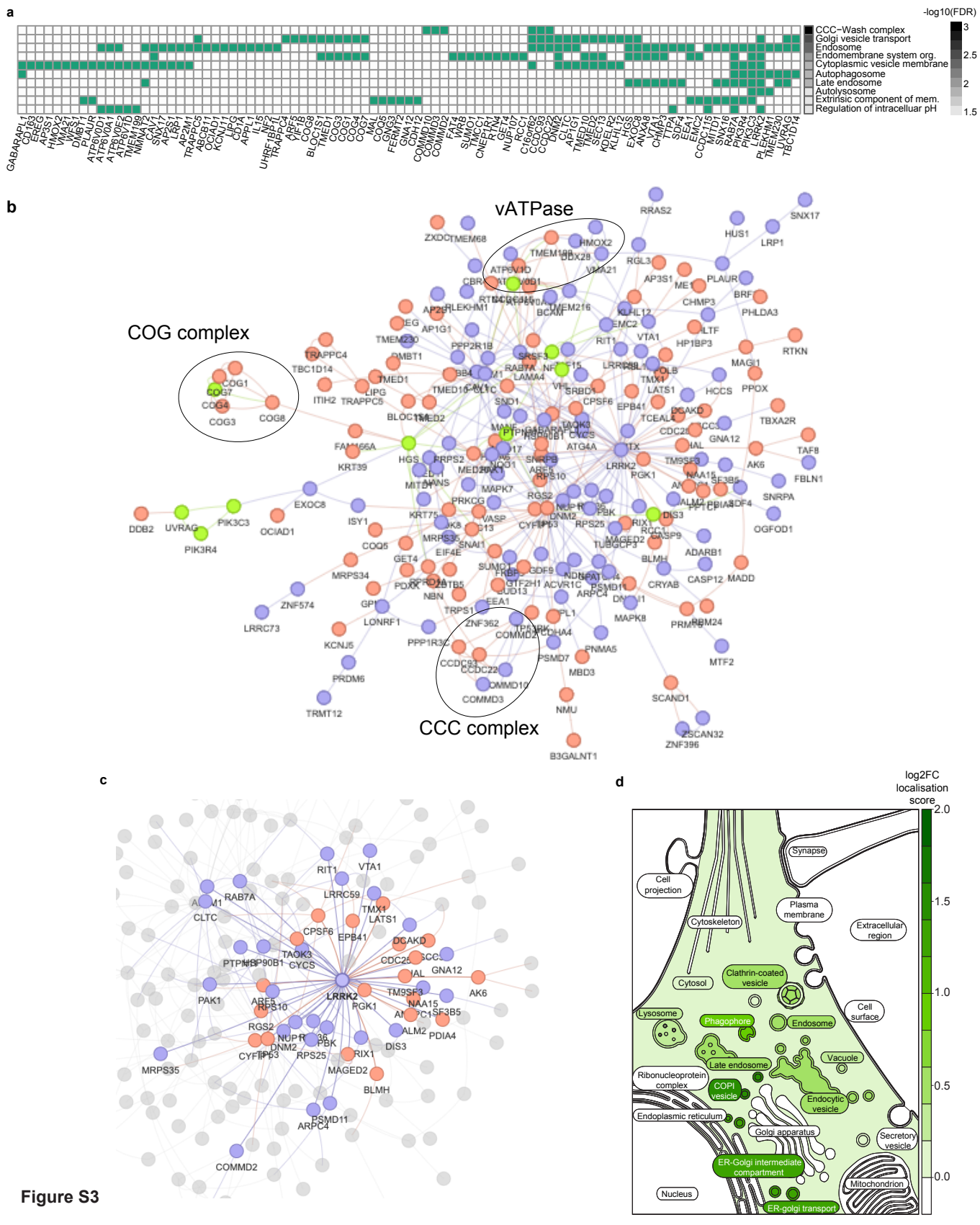
a
-log10(FDR)
3
2.5
2
1.5
CCC−Wash complex
Golgi vesicle transport
Endosome
Endomembrane system org.
Cytoplasmic vesicle membrane
Autophagosome
Late endosome
Autolysosome
Extrinsic component of mem.
Regulation of intracellular pH
b
vATPase
COG complex
CCC complex
c
d
log2FC
localisation
score
2.0
1.5
1.0
0.5
0.0
Synapse
Cell projection
Plasma membrane
Extracellular region
Cytoskeleton
Clathrin-coated vesicle
Cytosol
Cell surface
Lysosome
Phagophore
Endosome
Vacuole
Late endosome
Ribonucleoprotein complex
COPI vesicle
Endocytic vesicle
Endoplasmic reticulum
Golgi apparatus
Secretory vesicle
ER-Golgi intermediate compartment
Mitochondrion
Nucleus
ER-golgi transport

Figure S3

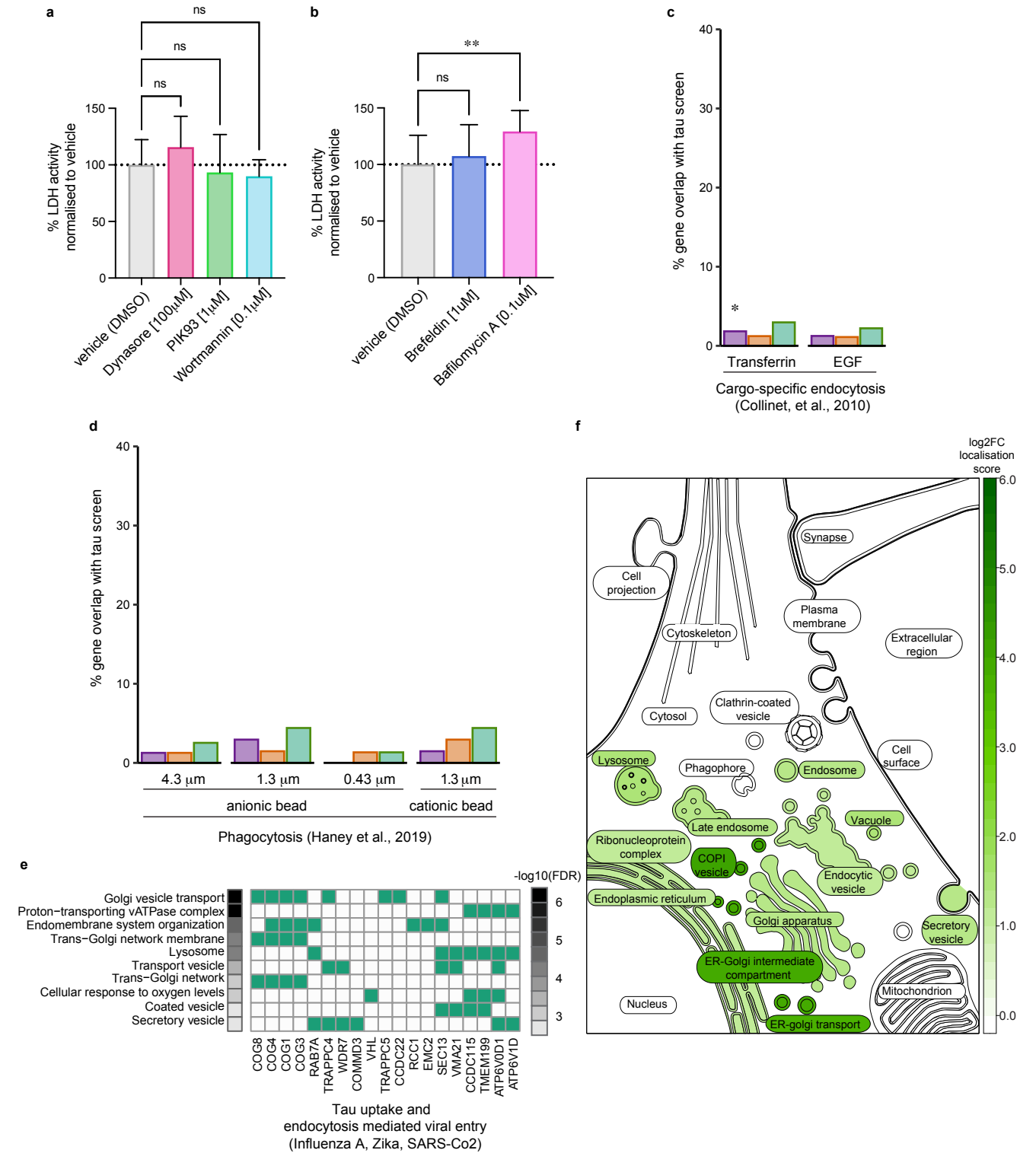
a
ns
ns
ns
% LDH activity normalised to vehicle
150
100
50
0
vehicle (DMSO)
Dynasore [100μM]
PIK93 [1μM]
Wortmannin [0.1μM]
b
**
ns
% LDH activity normalised to vehicle
vehicle (DMSO)
Brefeldin [1uM]
Bafilomycin A [0.1uM]
c
% gene overlap with tau screen
40
30
20
10
0
*
Transferrin
EGF
Cargo-specific endocytosis
(Collinet, et al., 2010)
d
% gene overlap with tau screen
4.3 μm
1.3 μm
0.43 μm
1.3 μm
anionic bead
cationic bead
Phagocytosis (Haney et al., 2019)
e
-log10(FDR)
Golgi vesicle transport
Proton−transporting vATPase complex
Endomembrane system organization
Trans−Golgi network membrane
Lysosome
Transport vesicle
Trans−Golgi network
Cellular response to oxygen levels
Coated vesicle
Secretory vesicle
COG8
COG4
COG1
COG3
RAB7A
TRAPPC4
WDR7
COMMD3
VHL
TRAPPC5
CCDC22
RCC1
EMC2
SEC13
VMA21
CCDC115
TMEM199
ATP6V0D1
ATP6V1D
Tau uptake and
endocytosis mediated viral entry
(Influenza A, Zika, SARS-Co2)
f
log2FC localisation score
Synapse
Cell projection
Plasma membrane
Cytoskeleton
Extracellular region
Clathrin-coated vesicle
Cytosol
Cell surface
Lysosome
Phagophore
Endosome
Late endosome
Vacuole
Ribonucleoprotein complex
COPI vesicle
Endocytic vesicle
Endoplasmic reticulum
Golgi apparatus
Secretory vesicle
ER-Golgi intermediate compartment
Mitochondrion
Nucleus
ER-golgi transport

Figure S4

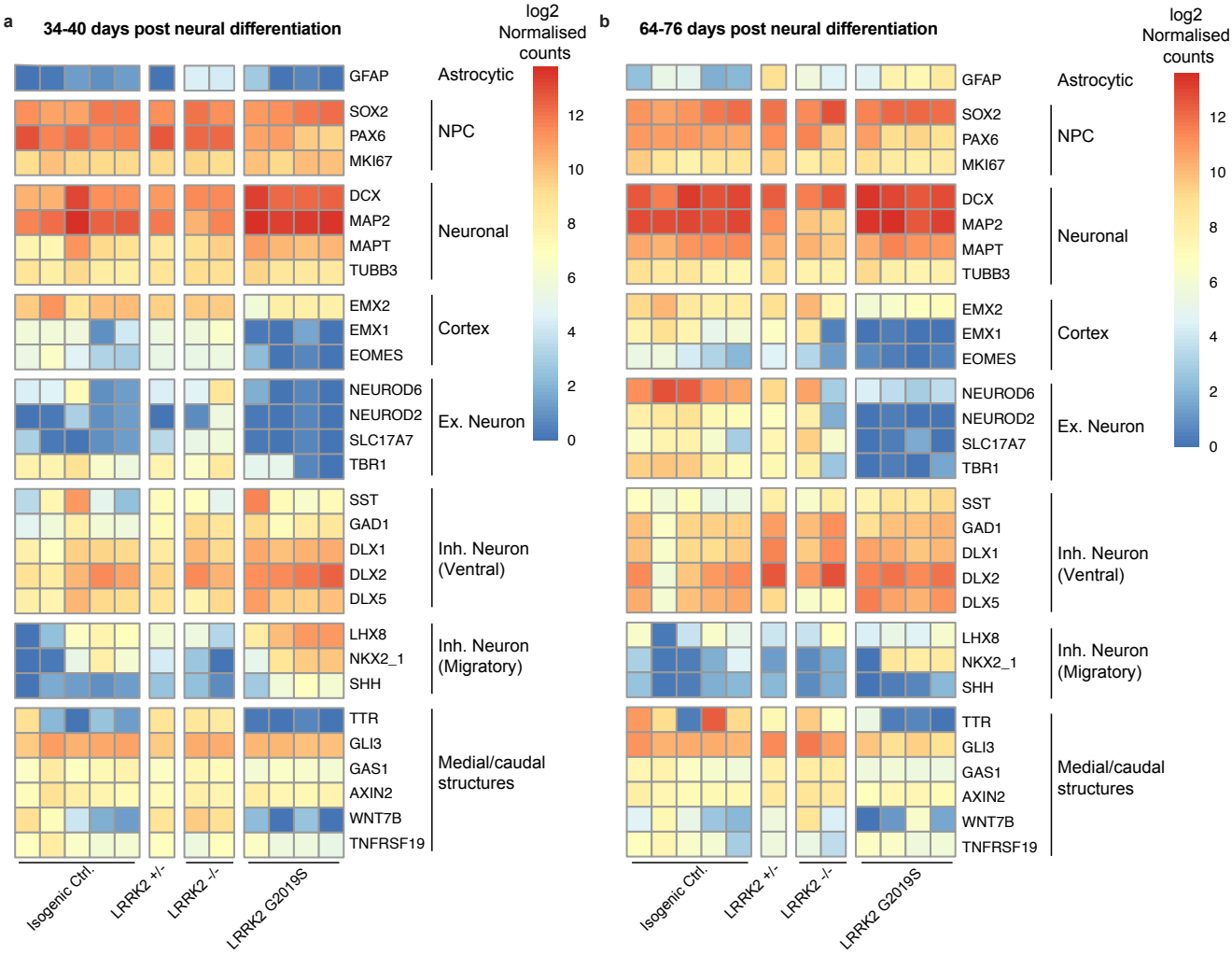
a
34-40 days post neural differentiation
b
64-76 days post neural differentiation
log2 Normalised counts
12
10
8
6
4
2
0
GFAP
Astrocytic
SOX2
PAX6
MKI67
NPC
DCX
MAP2
MAPT
TUBB3
Neuronal
EMX2
EMX1
EOMES
Cortex
NEUROD6
NEUROD2
SLC17A7
TBR1
Ex. Neuron
SST
GAD1
DLX1
DLX2
DLX5
Inh. Neuron (Ventral)
LHX8
NKX2_1
SHH
Inh. Neuron (Migratory)
TTR
GLI3
GAS1
AXIN2
WNT7B
TNFRSF19
Medial/caudal structures
Isogenic Ctrl.
LRRK2 +/-
LRRK2 -/-
LRRK2 G2019S

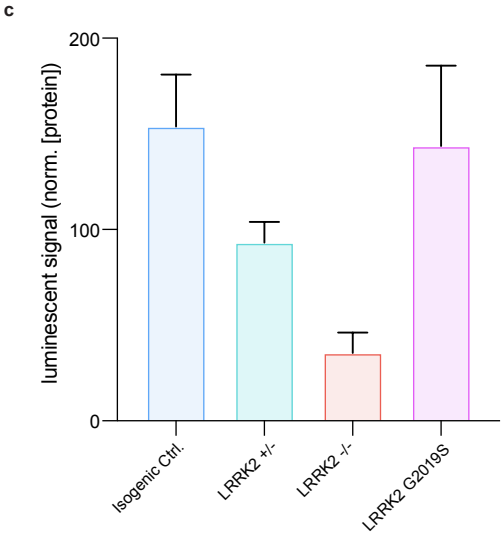
c
luminescent signal (norm. [protein])
200
100
0
Isogenic Ctrl.
LRRK2 +/-
LRRK2 -/-
LRRK2 G2019S

Figure S5

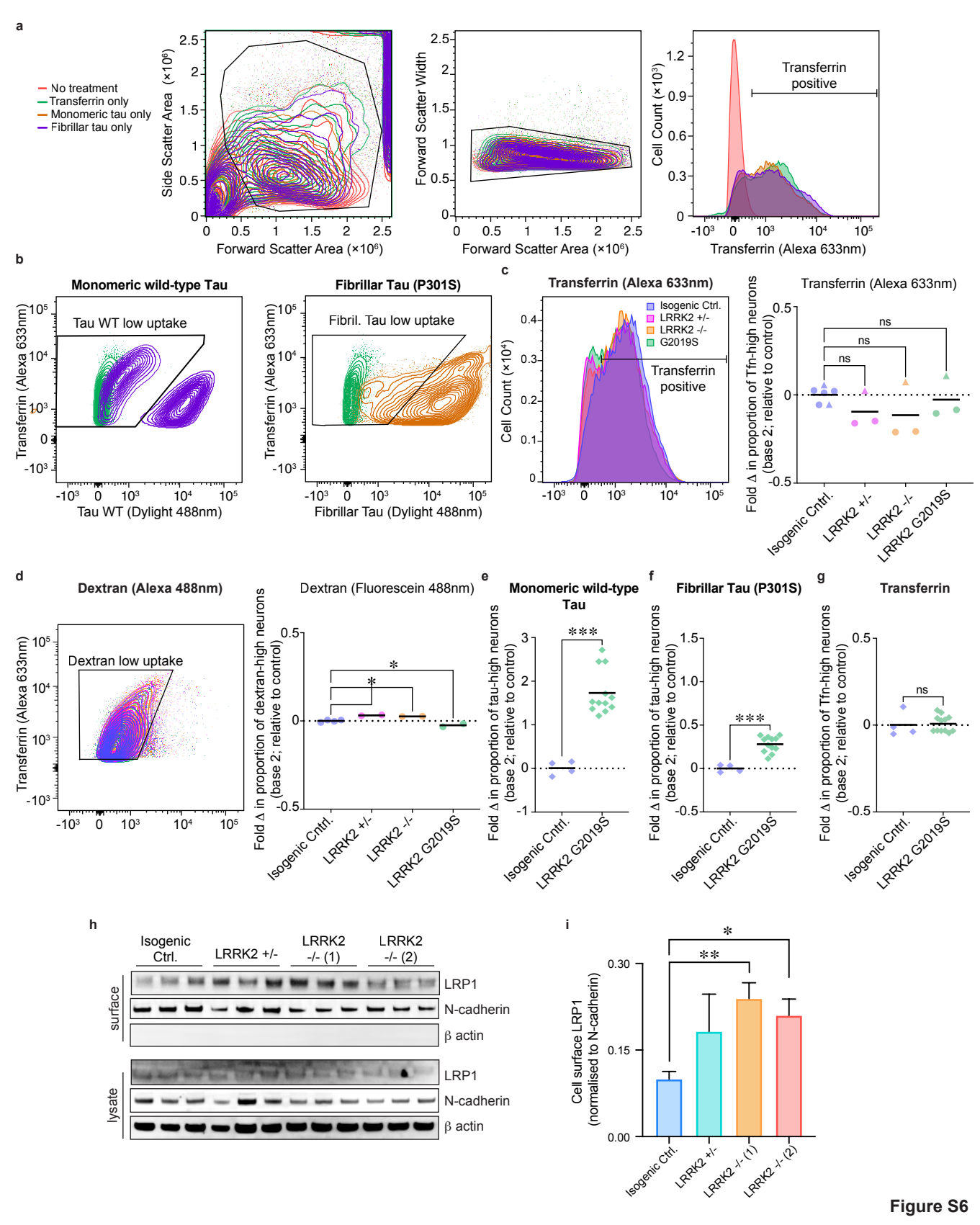
a
No treatment
Transferrin only
Monomeric tau only
Fibrillar tau only
Side Scatter Area (×10⁶)
Forward Scatter Area (×10⁶)
Forward Scatter Width
Cell Count (×10³)
Transferrin positive
Transferrin (Alexa 633nm)
b
Monomeric wild-type Tau
Tau WT low uptake
Tau WT (Dylight 488nm)
Fibrillar Tau (P301S)
Fibril. Tau low uptake
Fibrillar Tau (Dylight 488nm)
Transferrin (Alexa 633nm)
c
Transferrin (Alexa 633nm)
Isogenic Ctrl.
LRRK2 +/-
LRRK2 -/-
G2019S
Cell Count (×10⁴)
Transferrin positive
Fold Δ in proportion of Tfn-high neurons (base 2; relative to control)
ns
Isogenic Cntrl.
LRRK2 +/-
LRRK2 -/-
LRRK2 G2019S
d
Dextran (Alexa 488nm)
Dextran low uptake
Dextran (Fluorescein 488nm)
Fold Δ in proportion of dextran-high neurons (base 2; relative to control)
e
Monomeric wild-type Tau
Fold Δ in proportion of tau-high neurons (base 2; relative to control)
f
Fibrillar Tau (P301S)
g
Transferrin
h
Isogenic Ctrl.
LRRK2 +/-
LRRK2 -/- (1)
LRRK2 -/- (2)
surface
lysate
LRP1
N-cadherin
β actin
i
Cell surface LRP1 (normalised to N-cadherin)
LRRK2 -/- (1)
LRRK2 -/- (2)

Figure S6

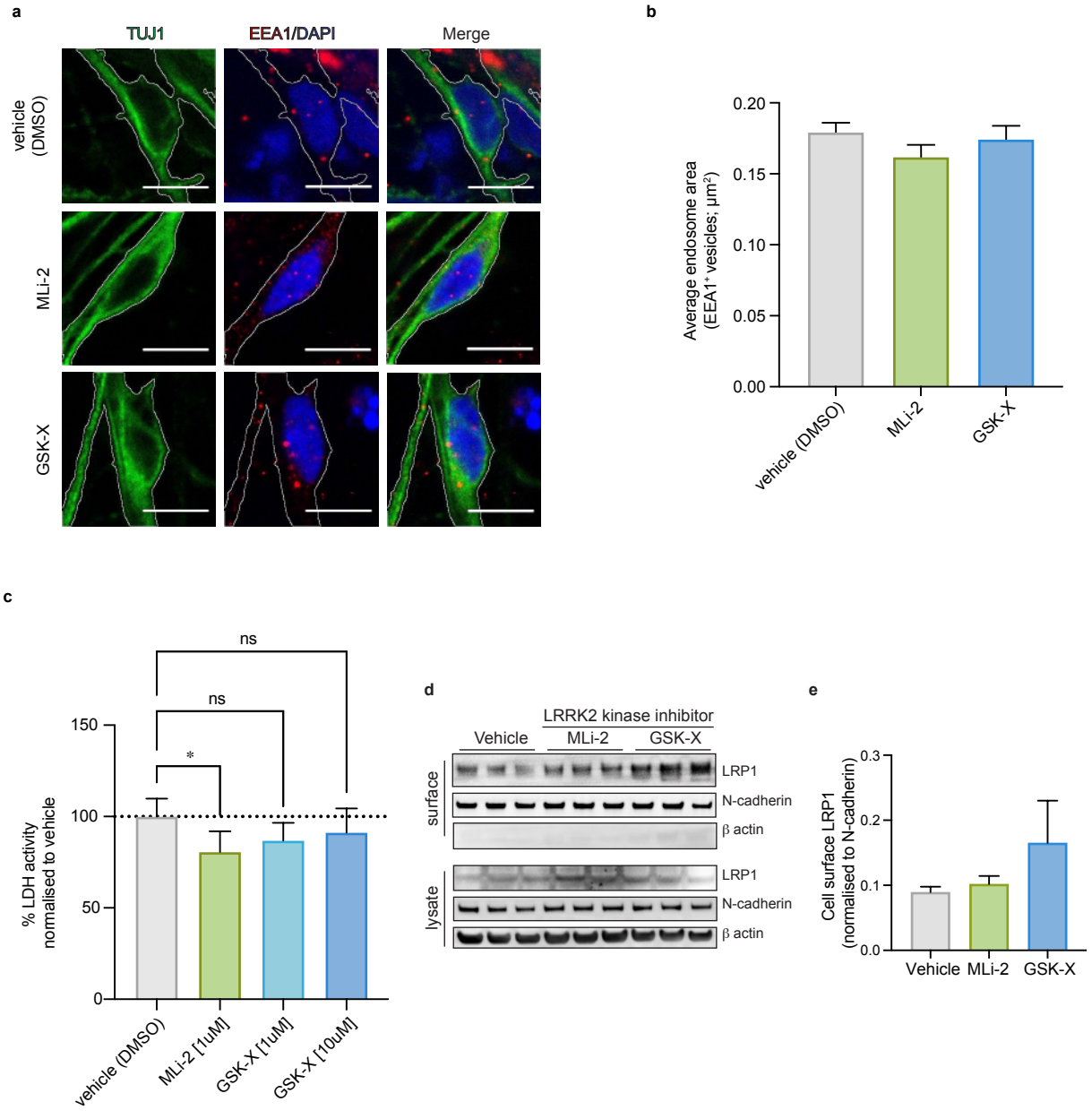
a
TUJ1
EEA1/DAPI
Merge
vehicle (DMSO)
MLi-2
GSK-X
b
Average endosome area (EEA1+ vesicles; µm2)
0.20
0.15
0.10
0.05
0.00
vehicle (DMSO)
MLi-2
GSK-X
c
ns
ns
*
150
100
50
0
% LDH activity normalised to vehicle
vehicle (DMSO)
MLi-2 [1uM]
GSK-X [1uM]
GSK-X [10uM]
d
LRRK2 kinase inhibitor
Vehicle
MLi-2
GSK-X
surface
lysate
LRP1
N-cadherin
β actin
LRP1
N-cadherin
β actin
e
Cell surface LRP1 (normalised to N-cadherin)
0.3
0.2
0.1
0.0
Vehicle
MLi-2
GSK-X

Figure S7